UNIVERSIDAD DE CONCEPCIÓN
FACULTAD DE INGENIERÍA
DEPARTAMENTO DE INGENIERÍA QUÍMICA

CFD-Based Studies and Model Development for Top-Blown Rotary Converters (TBRC)

POR

MAXIMILIANO ANTONIO SEPÚLVEDA IRARRÁZABAL

Memoria de Título presentada a la Facultad de Ingeniería de la Universidad de Concepción
para optar al título profesional de Ingeniero Civil Químico

Profesor Guía
Dr. Diego Becerra

Profesional Supervisor
Dr.-Ing. habil. Andreas Richter (TU Bergakademie Freiberg)

Enero, 2025
Concepción (Chile)

Affidavit

Resumen

Las simulaciones computacionales son una herramienta efectiva que permite estudiar fenómenos complejos con precisión, es especialmente útil en la investigación y creación de prototipos por su bajo costo económico y alta precisión. En el presente estudio se creó un modelo computacional de un reactor metalurgico TBRC a partir de un modelo TSL, ambos reactores son ampliamente utilizados en la industria de metales no ferrosos y asoman como opciones viables para el camino a la sostenibilidad. El objetivo del modelo computacional es estudiar el efecto de variables operacionales, como la velocidad de rotación y la inclinación, en el comportamiento hidrodinámico del sistema. En este tipo de reactores la interacción gas-líquido domina la velocidad de reacción y como consecuencia la eficiencia del proceso.

El modelo computacional es creado utilizando el software comercial Ansys FLUENT, para el seguimiento de la interfaz gas-liquido se utiliza el modelo "Volume of fluid (VOF)" el cual es acoplado con el modelo de turbulencia k-ω SST. Para estudiar el comportamiento hidrodinámico del sistema se analizan definiciones de informe, tales como el área total de la interfase gas-líquido, la frecuencia de burbujeo y la altura alcanzada por las gotas de liquido dentro del reactor junto con imágenes instantáneas y promediadas en el tiempo.

Los resultados revelan que la penetración de la lanza aumenta de gran manera la frecuencia de burbujas, además, se observa un aumento notable en el área total de interfase gas-liquido. Contrariamente a lo esperado, los patrones de recirculación tienden a ser más débiles a medida que aumenta la penetración, aumentando la probabilidad de zonas de estancamiento, sin embargo, la velocidad de rotación ayuda a mejorar la recirculación de los fluidos, en especial en la zona baja del reactor. La inclinación del reactor, una característica única de los reactores TBRC, disminuye la frecuencia de burbujas, el splashing y el área total de interfase gas-líquido, lo que resulta en una disminución en la interacción gas-líquido. Remover las zonas de estancamiento a traves del aumento en la velocidad de rotación y aumentar la penetración de la lanza para aumentar el area total de la inferface asegura que los reactivos esten en constante contacto con las superficies activas donde ocurren las reacciones, además, se facilitaria la transferencia de masa desde la fase gaseosa a la fase liquida, impactando directamente la conversión y la eficiencia del sistema.

Abstract

Computational simulations are an effective tool that allows for the precise study of complex phenomena; they are especially useful in research and prototype creation due to their low economic cost and high accuracy. In the present study, a computational model of a TBRC metallurgical reactor was created from a TSL model; both reactors are widely used in the non-ferrous metal industry and appear as viable options on the path to sustainability. The objective of the computational model is to study the effect of operational variables, such as rotation speed and inclination, on the hydrodynamic behavior of the system. In this type of reactors, the gas-liquid interaction dominates the reaction rate and consequently the process efficiency.

The computational model is created using the commercial software Ansys FLUENT. For tracking the gas-liquid interface, the "Volume of Fluid (VOF)" model is used, which is coupled with the k-ω SST turbulence model. To study the hydrodynamic behavior of the system, report definitions such as the total area of the gas-liquid interface, the bubbling frequency, and the height reached by the liquid droplets inside the reactor are analyzed, along with instantaneous and time-averaged images.

The results reveal that the lance penetration greatly increases the bubble frequency, and a notable increase in the total gas-liquid interfacial area is also observed. Contrary to expectations, the recirculation patterns tend to be weaker as penetration increases, increasing the likelihood of stagnant zones; however, the rotation speed helps improve fluid recirculation, especially in the lower zone of the reactor. The inclination of the reactor, a unique feature of TBRC reactors, decreases the frequency of bubbles, splashing, and the total gas-liquid interfacial area, resulting in a reduction in gas-liquid interaction. Removing stagnant zones through increased rotation speed and increasing the lance penetration to increase the total interface area ensures that the reactants are in constant contact with the active surfaces where the reactions occur. Additionally, it would facilitate mass transfer from the gaseous phase to the liquid phase, directly impacting the conversion and efficiency of the system.

Acknowledgments

First thanks to Professor Dr. habil. Andreas Richter for introducing me to Computational Fluid Dynamics and for giving me the opportunity to write my thesis with him. Second thanks to Preetam for always being available and helping me as much as possible. Third, thanks to my family, the fundamental pillar of my life and finally thanks to Professor Dr. Diego Becerra, without him this would not have been possible.

Contents

List of Figures

List of Tables

1 Introduction

In an era where global warming is alarming and CO_2 levels in the atmosphere are at unprecedented levels [1], industrial innovation is focused on reducing CO_2 emissions and making industrial processes cleaner and more energy efficient [2]. One industry that is of great concern because of its high CO_2 emissions, high energy consumption and extensive use of fossil fuels is the metallurgical industry. This industry produces at least 7% of the total global CO_2 emissions and to meet the large energy requirement it uses mostly fossil fuels, specifically, the energy used in the production of steel and aluminum comes from 83% and 62% of fossil fuels, respectively [3–6].

The metallurgical industry can be divided mainly into the production of ferrous metals, i.e. iron and its alloys and the production of non-ferrous metals such as aluminum and copper [7]. Within the production of non-ferrous metals, different metallurgical processes are used, such as pyrolysis in which high temperatures are used to extract and purify metals from their ores, concentrates or electronic waste. Pyrolysis and other processes are based on thermal reactions such as fusion, reduction, oxidation and other treatments involving different states of matter, i.e. processes involving gases, liquids and solids in the same system [8].

Tin (Sn) is a non-ferrous metal widely known for its corrosion resistance, malleability and low melting point, these characteristics position it as an excellent choice for corrosion prevention and it is widely used in tin-plating, food packaging and soldering [7]. However, tin production faces two major challenges: (1) the difficulty in separating iron oxide, Fe_2O_3, without affecting metal recovery, and (2) process inefficiencies resulting from equipment design. The first comes from the similarity in physical properties between iron oxide and tin oxide and the second from inefficiencies in heat propagation, which results in exaggerated energy consumption and heat losses leading to high energy demand and high operational cost [9–11].

Among the technologies implemented to address these challenges, the Top-Submerged Lance (TSL) technology and the Top-Blown Rotary Converter (TBRC) have emerged as critical solutions [9, 12, 13]. TSL technology, a bath smelting process, utilizes a vertical cylindrical furnace with a central lance submerged in the slag bath. The lance injects fuel and air, creating bubbles that rise through the melt [14] and thus turbulence, which facilitates efficient mass and heat exchange between the phases, enhancing reaction rates and process efficiency [13]. TSL technology is also highly versatile, capable of processing a wide range of raw materials, such as concentrates, secondary materials, and by-products. TSL technology is currently used to produce 55% of the world's tin, and all TSL smelters comprised have the installed capacity to process more than half mined copper worldwide [14].

The TBRC technology, unlike the TSL, blows gas through a not submerged-lance directly onto the melted bath, and it also integrates a rotation system for the entire reactor. This rotational movement ensures constant mixing, prevents crust formation on the walls, and significantly enhances heat transfer and reaction rates [13]. The TBRC excels in refining and recovering valuable metals from complex feedstocks, such as electronic waste or slag. Its design allows precise control over operating conditions, achieving high recovery rates while minimizing energy losses [12].

Hydrodynamics is a branch of physics that deals with the motion of fluids [15], specifically in bath smelting reactors hydrodynamics describes the behavior of molten metal, slag and gas phases. In TBRC and TSL reactors hydrodynamics is linked to critical phenomena such as flow patterns, phase mixing, and heat and mass transfer [16]. The importance of hydrodynamics in the efficiency of these high-temperature reactors lies in the fact that smelting reactions occur at the gas-liquid interface [17]. A larger interfacial area provides more surface for the reactants to interact and react effectively. This interface is strongly influenced by liquid splashing and bubble dynamics. In addition, intense agitation and bubble dynamics generate flow patterns within the reactor, promoting fluid motion and eliminating stagnant zones. These stagnant areas could produce explosions if they contain unburned fuel [18].

Many publications and studies have focused on the study of these metallurgical reactors separately, but there is still a shortage of studies that combine the key TBRC characteristics, such as rotational speed and inclination angle, into TSL models. Combining both technologies could lead to an efficient alternative for enhanced reaction rates and energy efficiency. For instance, Obiso *et al.* [19] studied the influence of lance immersion depth and gas flow rate in a TSL reactor, highlighting the impact of these parameters on hydrodynamic phenomena such as turbulence and mixing. Regarding TBRC technology, Pérez-Tello *et al.* [20] and Huang *et al.* [21], revealed how gas flow rate, rotation speed, and inclination angle affect hydrodynamic variables such as mixing efficiency and splashing height.

To address this gap, the present study builds upon experimental and computational work conducted at the Institute of Nonferrous Metallurgy and High Purity Materials (INEMET) and the Institute of Energy Process Engineering and Chemical Engineering (IEC), respectively, at TU Bergakademie Freiberg. The experiments at INEMET melted and reduced a concentrated SnO_2 slag using hydrogen, converting SnO_2 into SnO within a cylindrical corundum vessel in an induction furnace in order to replicate TSL reactor conditions. The goal of these experiments was to study the reduction of SnO_2 using hydrogen. These experimental studies were extended by Voigt [22] by developing a computational model to capture liquid-gas interface behavior and analyze hydrodynamics and reaction dynamics.

Studying the hydrodynamics of multiphase fluids is difficult because the phases interact non-linearly, droplets and bubbles form, temperature and concentration gradients arise, and moreover, multiphase systems are highly dynamic, meaning they change rapidly in space and time. The study of multiphase flows in metallurgical reactors is even more complex given the high temperatures that make it impossible to introduce cameras inside the reactors. Additionally, the flows are highly turbulent and the chemical reactions generate toxic gases [13, 17].

Computational Fluid Dynamics (CFD) has emerged as a cornerstone in unraveling these complexities [16, 19, 23]. CFD, a branch of fluid mechanics, is a powerful tool for detailed flow analysis. It uses algorithms and numerical techniques to solve and investigate problems involving fluid flow. Due to the rapid increase in computational power, CFD can increasingly simulate more complex conditions and at a greater speed. This, combined with its low cost and high accuracy, has made CFD an indispensable tool in various industries such as automotive and aerospace [24].

This thesis builds upon the computational model presented in the work of Voigt [22], which was initially developed for a TSL experimental model. The existing model has been modified and the unique features of TBRC technology, i.e., rotational motion and inclination, have been added to it. Furthermore, this work investigates the influence of these TBRC parameters, along with lance immersion depth and gas flow rate, on critical hydrodynamic phenomena, including turbulence, bubble frequency, and the gas-liquid interface. This study belongs to a wider study that the group of Modeling of Thermochemical Conversion Processes (MTK), part of the Institute of Energy Process Engineering and Chemical Engineering (IEC), is conducting. Addressing this gap will lay the foundation for future research that will integrate the hydrodynamics of a TBRC-TSL system with chemical reactions. Thus, this research contributes to the broader goal of optimizing bath smelting reactors to enhance energy efficiency, reduce operational costs, and finally achieve sustainability in the non-ferrous metal industry.

The following of this study presents the Fundamentals of Computational Fluid Dynamics, the description of the previous experimental model, its extension to a computational model, the extended computational model, the tracked parameters and a detailed discussion of a parameter study performed on the TBRC-TSL computational model.

1.1 Theoretical Background

1.1.1 Introduction to TSL and TBRC Reactors

Mainly used for smelting, refining and recovery of non-ferrous metals, these reactors are based on the injection of a high gas flow that interacts with the slag generating turbulence, agitation and a large liquid-gas interface that enhances reaction rates. Aurubis AG, the world's largest non-ferrous metal recycling company [25], employs both types of reactors in its renowned "Kayser Recycling System [26]." This process allows them to produce over 18,000 tons of copper and 5,000 tons of tin annually.

1.1.2 Top Submerged Lance (TSL) Reactor

Developed in the early 70's, the TSL technology is based on a vertically positioned cylindrical furnace in which a lance is introduced from the top to the inside of the liquid bath, through this lance a large quantity of gas is introduced which interacts violently with the liquid bath favoring the mixing and the speed of the chemical reactions (Figure 1.1). In addition, these reactors can process different types of raw materials such as concentrates or electronic waste [14]. Despite its advantages TSL reactors still face challenges such as rapid wear of the lance and the reactor's internal lining. This phenomenon has been closely linked to gas flow rate, lance positioning, and the reactor's hydrodynamics [13, 23].

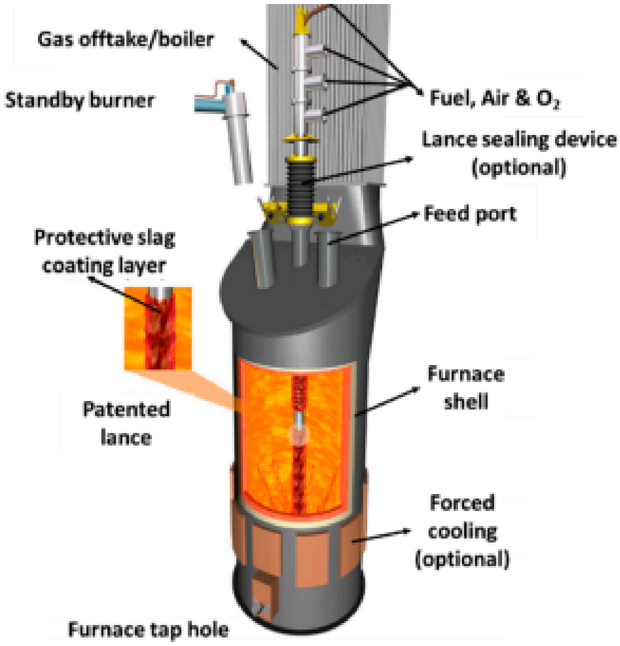

Figure 1.1: AUSMELT reactor scheme. The lance enters from the top of the reactor until it is submerged in the metal bath, which has different openings that allow the entry of fuel, air and oxygen. The reactor has feed inlets at the top and also an exhaust gas outlet. Adapted from [14].

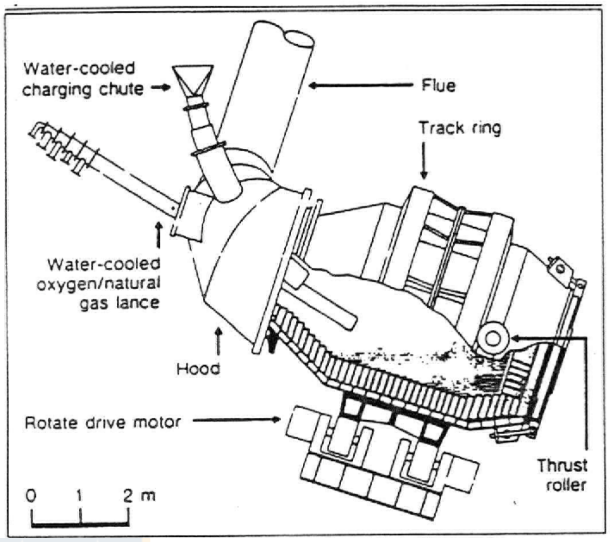

Figure 1.2: TBRC scheme. The reactor has a "Thrust roller" in charge of tilting the reactor and a motor that rotates it. The lance is introduced from the top and allows injecting the reagents. The reactor has a gas outlet at the top. Adapted from [13].

1.1.3 Top-Blown Rotary Converter (TBRC) Reactor

The Top-Blown Rotary Converter (TBRC) reactors emerged as a technological evolution of the Kaldo converter, developed in the 1950s and designed for metal refining and electronic waste recycling, these reactors operate at high temperatures, which is necessary to produce the molten metal bath [13].

One of the main characteristics of TBRC technology is the top-blowing of the reaction gases onto the metal bath, unlike Top-Submerged lance (TSL) technology where the gas is injected directly into the metal bath. The other two unique characteristics of TBRC technology are the rotation and inclination systems, which can be seen in Figure 1.2. These features improve mixing efficiency and are necessary to remove both the desired and undesired products [17].

2 Objectives

2.1 General objective

Combine the main characteristics of TSL technology and TBRC technology and develop a computational model in order to study the hydrodynamic behavior under different operational parameters modifications.

2.2 Specific objectives

1. **Use the TSL computational model developed previously and add inclination and rotation in order to replicate TBRC technology.**
2. **Modify the position of the lance through a computational remeshing**
3. **Analyze the effects of the following parameters on this system:**
    - Mass flow rate of the gas.
    - Rotational speed of the crucible.
    - Lance position.
4. **Analyze the effect of different angles α keeping the previous parameters constant.**

3 Simulation model and methodology

3.1 Overview of Computational Fluid Dynamics

Computational fluid dynamics (CFD) corresponds to a confluence of fluid mechanics, engineering, computer science, and numerical analysis, and it allows for the prediction of fluid behavior and development in multiple scenarios. Computational fluid dynamics is a tool used in various industries such as automotive, aerospace, and aeronautics with the aim of predicting behaviors, optimizing designs, reducing costs, and improving performance. CFD softwares provide visualization options for flow patterns, pressure drops, flows and temperature distribution, multiphase fluid interfaces, and particle paths [24].

3.2 Fundamentals of Computational Fluid Dynamics

Computational Fluid Dynamics (CFD) is based on the numerical solution of the Navier-Stokes equations, which govern the motion of fluid flows [15]. These equations express the conservation of mass, momentum, and energy in a fluid:

3.2.1 Conservation of Mass (Continuity Equation)

$$\frac{\partial \rho}{\partial t} + \nabla \cdot (\rho \mathbf{v}) = 0 \tag{3.1}$$

Where ρ is the fluid density, t is the time, $\mathbf{v}$ is the velocity vector and $\nabla\cdot$ is the divergence of a vector field.

3.2.2 Conservation of Momentum (Navier-Stokes Equations)

$$\rho \frac{\partial \mathbf{v}}{\partial t} + \rho(\mathbf{v} \cdot \nabla)\mathbf{v} = -\nabla p + \mu \nabla^2 \mathbf{v} + \mathbf{F} \tag{3.2}$$

Where p is the pressure, μ is the dynamic viscosity, ∇^2 is the Laplacian operator (diffusion) and $\mathbf{F}$ accounts for body forces (e.g., gravity).

3.2.3 Conservation of Energy

$$\rho \frac{\partial e}{\partial t} + \nabla \cdot (\rho \mathbf{v} e) = -\nabla \cdot \mathbf{q} + \Phi \tag{3.3}$$

Where e is the specific internal energy, $\mathbf{q}$ is the heat flux and Φ accounts for energy dissipation terms (e.g., due to viscosity).

3.2.4 CFD methodology

The conservation equations are solved using numerical methods, for which there are various methods; the most common is the finite volume method, which discretizes the equations in a computational domain by approximating the derivative terms to algebraic equations. Depending on the problem, it is necessary to solve other equations to capture critical phenomena such as turbulence or multiphase fluids. Simulations accuracy depends on the chosen numerical models, the mesh resolution and the problem setup [24].

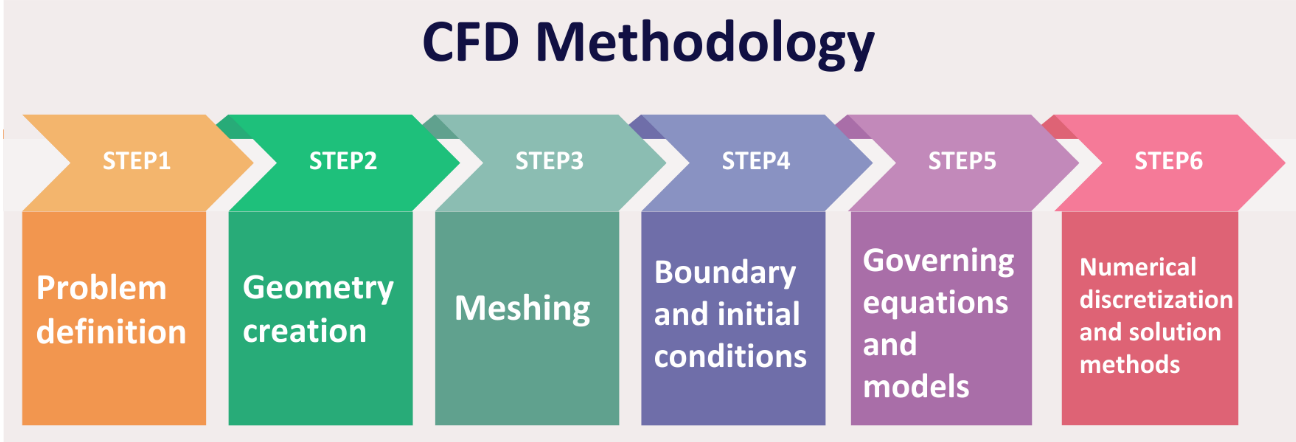

Figure 3.1: CFD Methodology.

3.2.5 Volume of Fluid Model (VOF)

The volume of fluid (VOF) method is one of the most common methods for simulating multiphase flows. The VOF method is an interface capturing method in an Eulerian framework. The method is based on the idea of a so-called fraction function which is a scalar function, defined as the integral of a fluid's characteristic function in the control volume, namely the volume of a cumputational grid cell. The volume fraction of each fluid is tracked through every cell in the computational grid [27]:

$$\alpha = \begin{cases} 0 & \text{, The cell is only gas,} \\ 1 & \text{, The cell is only liquid,} \\ 0 < \alpha < 1 & \text{, At the interface.} \end{cases} \tag{3.4}$$

Based on α value the interface is reconstructed using an approximation scheme. The Geometric Reconstruction Scheme applied in this model uses a Piecewise-Linear Interface Construction (PLIC) approach, which calculates the normal vector of the interface. Once the reconstruction process of the interface is done, it must be ensured that the volume fraction of each fluid α is updated correctly as the flow moves through the computational cells. For this, the volume fraction advection equation is used, which describes how alpha changes in space and time due to the movement of the fluid.

$$\frac{\partial \alpha}{\partial t} + \nabla \cdot (\alpha \mathbf{v}) = 0. \tag{3.5}$$

These two steps are therefore performed at each time step and allow the interface to be tracked over time. The VOF model belongs to the so-called one-fluid models, in which only one set of the governing equations is solved [27]. Then, for an incompressible multiphase flow:

$$\nabla \cdot \mathbf{v} = 0. \tag{3.6}$$

$$\frac{\partial \rho(\alpha)\mathbf{v}}{\partial t} + \nabla \cdot (\rho(\alpha)\mathbf{v}\mathbf{v}) = -\nabla p + \nabla \cdot \mu(\alpha)\left[\nabla \mathbf{v} + (\nabla \mathbf{v})^T\right] + \mathbf{f}_g + \mathbf{f}_\sigma \tag{3.7}$$

Where $\rho(\alpha)$ is the density as a function of the volume fraction α, $\mu(\alpha)$ is the dynamic viscosity as a function of α, $\mathbf{f}_g$ is the body force due to gravity, $\mathbf{f}_\sigma$ is the surface tension force.

In this model the local fluid properties of density and viscosity are defined as a function of the local volume fraction:

$$\rho(\alpha) = \rho_l \alpha + \rho_g (1 - \alpha) \tag{3.8}$$

$$\mu(\alpha) = \mu_l \alpha + \mu_g (1 - \alpha) \tag{3.9}$$

Where α is the volume fraction, ρ_l is the density of the liquid phase, ρ_g is the density of the gas phase, μ_l is the dynamic viscosity of the liquid phase, μ_g is the dynamic viscosity of the gas phase.

Due to the turbulence inside the reactor the equations 3.6 and 3.7 cannot be solved directly due to rapid and chaotic flow fluctuations. Therefore a turbulence model is needed which is explained in the next section.

3.2.6 Turbulence Model

Turbulent flows are characterized by having a chaotic and changing behavior through space and time, with the aim of representing this behavior the velocity $\mathbf{v}$ is decomposed into a mean component, $\overline{\mathbf{v}}$, and a fluctuating component, $\mathbf{v}'$, as:

$$\mathbf{v} = \overline{\mathbf{v}} + \mathbf{v}'.$$

Substituting this decomposition into the momentum equations and averaging introduces additional terms, known as the Reynolds stresses ($\rho\overline{\mathbf{v}'\mathbf{v}'}$). These stresses represent the momentum transport due to turbulence and must be modeled to "close" the system of equations.

The viscous term in the momentum equation is modified to include an effective viscosity:

$$\mu_{\text{eff}} = \mu(\alpha) + \mu_t,$$

Where μ_t is the turbulent viscosity. For the k-ω SST (Shear Stress Transport) model, this viscosity is determined by solving two additional transport equations: one for the turbulent kinetic energy (k) and another for the specific dissipation rate (ω)[24].

Turbulent kinetic energy equation

$$\frac{\partial \rho(\alpha) k}{\partial t} + \nabla \cdot \rho(\alpha) k \vec{v} = \nabla \cdot \left[\left(\mu(\alpha) + \frac{\mu_t(\alpha)}{\sigma_k} \right) \nabla k \right] + G_k - Y_k, \tag{3.10}$$

Specific dissipation rate equation

$$\frac{\partial \rho(\alpha) \omega}{\partial t} + \nabla \cdot \rho(\alpha) \omega \vec{v} = \nabla \cdot \left[\left(\mu(\alpha) + \frac{\mu_t(\alpha)}{\sigma_\omega} \right) \nabla \omega \right] + G_\omega - Y_\omega. \tag{3.11}$$

$$\mu_t = \frac{\rho(\alpha) k}{\omega} \cdot \frac{1}{\max\left(1, \frac{S F_2}{a_1}\right)}, \tag{3.12}$$

$$F_2 = \tanh(\Phi_2^2), \tag{3.13}$$

$$\Phi_2 = \max\left[\frac{\sqrt{k}}{0.09 \omega y}, \frac{500 \mu}{\rho(\alpha) \omega y^2} \right]. \tag{3.14}$$

Where ρ is the mixture density, α is the phase volume fraction, k is the turbulence kinetic energy, ω is the specific dissipation rate, $\mu(\alpha)$ is the dynamic viscosity as a function of phase fraction, μ_t is the turbulent viscosity (Eq. 3.12), σ_k, σ_ω are turbulence Prandtl numbers for k and ω, G_k, G_ω are the production terms for k and ω, Y_k, Y_ω are the dissipation terms for k and ω, S is the mean strain rate, y is the distance to the nearest wall, F_2 is the blending function (Eq. 3.13), Φ_2 is a parameter for wall damping (Eq. 3.14) and a_1 is a model constant.

The k-ω SST turbulence model is used in this work because it combines the accuracy of the k-ω model near the walls with the stability of the k-ϵ model in the free stream. Then the viscous term results in:

$$\nabla \cdot \left[\mu_{\text{eff}} \left(\nabla \mathbf{v} + (\nabla \mathbf{v})^T \right) \right]. \tag{3.15}$$

where μ_{eff} now accounts for both molecular and turbulent viscosity. The accounting of these 2 effects is fundamental for a correct modeling of turbulence, especially in the presence of complex, chaotic flows and complex geometries. Under these conditions, the k-ω SST model is the optimal and chosen model.

3.3 Previous work

This work is based on experiments carried out at the Institute for Non-Ferrous Metallurgy and Pure Materials (INEMET) at TU Bergakademie Freiberg where the reduction of cassiterite using hydrogen as reducing agent was studied, this experiment was then reproduced by a numerical model which served as the basis for the present work.

3.3.1 The Experimental Setup

In order to study the reduction of tin dioxide (SnO_2) to tin oxide (SnO) using hydrogen, two experiments were carried out using a 15-centimeter long cylindrical corundum crucible (Figure 3.2. (a)) containing a lance submerged at the top. A cassiterite concentrate was introduced into the crucible and subsequently melted in an induction furnace at 1300°C while hydrogen was blown through the lance into the melt. Hydrogen was constantly supplied which produced a reducing atmosphere inside the crucible. The experiments had a duration of 6.7 and 13.4 hours. The configuration of these experiments corresponds to a scaled-down configuration of a TSL industrial reactor.

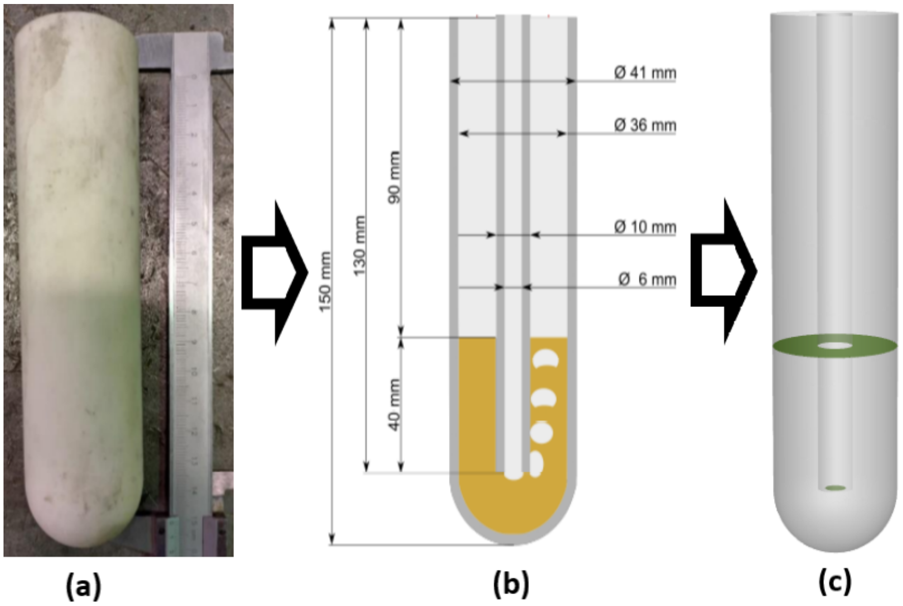

Figure 3.2: Scheme of the transition from the experimental model to the computational model: (a) Crucible used for the experiments, the crucible is 15 cm long made of corundum, (b) Scheme of the physical dimensions of the crucible, the crucible has a diameter of 4.1 cm and the lance of 1 cm, the mustard zone corresponds to the slag and the raising bubbles correspond to the hydrogen encapsuled by the slag, (c) Computational model of the crucible, the green zone corresponds to the initial gas-liquid interface.

3.3.2 Computational model

To study the relationship between the hydrodynamics of the gas-liquid system and the reduction reactions, the experiment was reproduced in the work of Voigt [22] using the commercial software Ansys Fluent. A 330,000 cell computational grid was created to exactly replicate the physical dimensions of the experiment (Figure 3.2: (b)). For the tracking of the gas-liquid interface the Volume of Fluid model (Section 3.2.5) was used, this model is ideal for capturing interfaces between immiscible fluids and is especially suitable for problems where accuracy in the description of the interface shapes is required. The VOF model was coupled to the k-ω SST turbulence model (Section 3.2.6.).

3.4 TBRC Computational model

It should be noted that the previous computational model was developed by Voigt [22] to study the interactions between the chemical reaction and the system hydrodynamics, simulating the experiment described in the previous section. However, the objective of this thesis is not to study the chemical reaction but rather the hydrodynamic behavior of the multiphase fluid under a TBRC setup and how operational parameters affect this behavior. Therefore, the chemical reaction is not considered, assuming two non-reactive fluids that retain their fundamental properties.

3.4.1 Ansys Fluent

The software used to perform the simulations is Ansys Fluent, a CFD solver that allows to simulate and analyze the behavior of fluids, heat flows, chemical reactions and other physical phenomena. Ansys Fluent allows the user to select different physical models, numerical methods, solvers, convergence criteria and track different properties over time. Once the setup is configured, Ansys Fluent solves the governing equations (Section 3.2) until reaching convergence. Then in post-processing, the program offers different visualization tools and generates plots, contours, animations and quantitative data [28].

3.4.2 Rotation

The first step in order to replicate the TBRC behavior is rotating the wall. This feature is unique of Top-Blown Rotary Converters and depends on the reactor size, the smaller the volume of the reactor, the higher the rotation speed. For real industry TBRC the following data could be obtained [29]:

Table 3.1: Relationship between reactor´s volume and rotation speed.

Reactor´s volume (m^3)	**Rotation speed (RPM)**
0.8	20
4	16
20.0	12

With the data obtained, an inversely proportional relationship is created between the reactor volume (m^3) and the rotation speed (RPM).

$$\text{RPM} = C \cdot V^{-k} \tag{3.16}$$

Where C is a constant and k is an exponent that is determined from the data.

Applying the data in Table 3.1, the system of equations can be solved to determine C and k. This adjustment was performed numerically using Python and the least squares method. The following values for the parameters are obtained from the adjustment:

$$C = 19.44\,\mathrm{RPM}\cdot\mathrm{m}^{0.465}, \quad k = 0.155 \tag{3.17}$$

Therefore, the relationship between the reactor volume and the rotational speed is given by:

$$\text{RPM} = 19.44\,\mathrm{RPM}\cdot\mathrm{m}^{0.465}\cdot V^{-0.155} \tag{3.18}$$

The volume of the crucible (Figure 3.4) is $1.445 \times 10^{-4}\,\mathrm{m}^3$, therefore:

$$\text{RPM} = 19.44\cdot(0.0001445)^{-0.155} \approx 76.75 \tag{3.19}$$

However, when using this value in the simulations, hydrodynamic parameters such as the height of the splashing and the bubble frequency changed slightly. This may be attributed to the fact that the data obtained in Table 3.1 are for TBRC reactors where the lance is not introduced into the slag as in a TSL reactor. This change affects the real volume available to the fluids within the reactor. Therefore, the rotation speed is set to 95.5 RPM.

3.4.3 Inclination

The second step is to tilt the crucible, this feature is fundamental in TBRC reactors since it is related to splashing, mixing efficiency and reactor life [20, 21]. The initial angle of inclination used is 45° with respect to the horizontal.

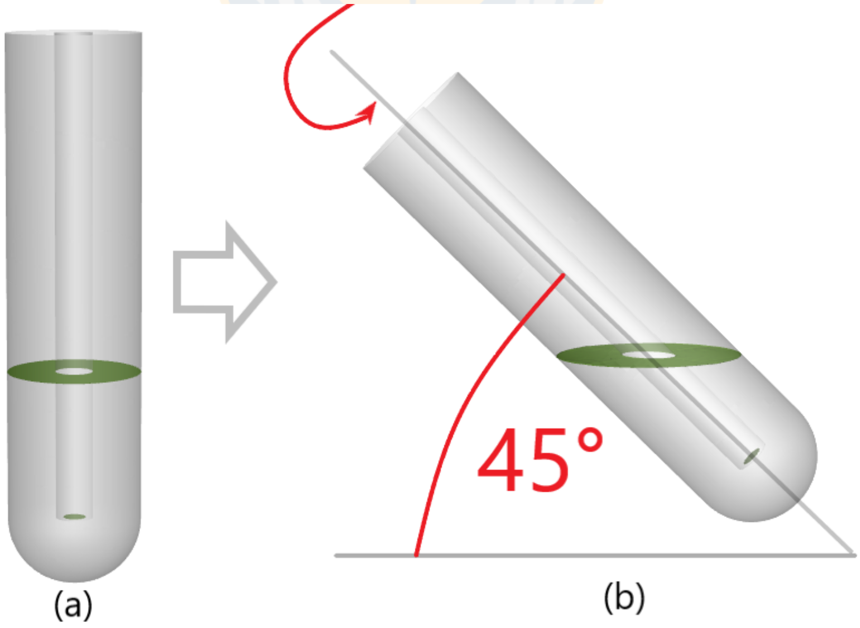

Figure 3.3: Tilting and rotating the computational TSL model: (a) Previous computational model (TSL), (b) TBRC computational model.

3.4.4 Setup summary

The computational model for a TBRC is shown in Figure 3.3(b). The following tables summarize the model characteristics, the fluid properties and the numerical configuration used for the simulations.

Table 3.2: Operational parameters and physical properties

Parameter	**Value**	**Parameter**	**Value**
Rotation speed (ω, rpm)	95.5	Slag viscosity (μ_l, kg/m s)	0.2
Inclination (θ, degrees)	45	Slag density (ρ_L, $\mathrm{kg/m^3}$)	5600
Mass flow rate ($\dot{m}$, kg/s)	2.152×10^{-5}	Gas density (ρ_G, $\mathrm{kg/m^3}$)	0.3
Lance penetration depth (d/D)	0.867	Surface tension (σ, N/m)	0.55

Table 3.3: Numerical setup

Solver	**3D transient**
Models	VOF explicit Continuum Surface force model k-ω SST turbulence model
Numerical methods	Pressure-velocity coupling: SIMPLE Momentum: QUICK Pressure: PRESTO! Volume fraction: GEO-Reconstruct
Discretization	Δx: $3 \times 10^{-4}\,\mathrm{m}$ Δt: $1 \times 10^{-5}\,\mathrm{s}$

3.5 Parametric Study

The impact of operational parameters on the hydrodynamics of bath smelting reactors has been extensively studied over the past decade and it has been proven that they have a significant effect on it. Given that the hydrodynamics of bath smelting reactors directly affects the reaction kinetics and thereby the overall efficiency of the process, operational parameters are an area of key focus. In the following paragraphs the parameters to be modified are indicated [16, 18–21, 30].

3.5.1 Gas flow rate

In both TSL and TBRC reactors, gas flow serves two main purposes: delivering reactants (e.g., oxygen for oxidation or hydrogen for reduction) and maintaining the desired atmosphere for efficient reactions. Additionally, inert gases (e.g., Nitrogen or Argon) enhance mixing, heat and mass transfer, and reactant distribution. In TSL reactors, gas injection into the molten bath creates intense bubbling, while in TBRC reactors, gas blown over the surface relies on reactor rotation for mixing [12, 14, 31].

3.5.2 Lance position

The position of the lance is a key factor in both TSL and TBRC technologies. In TSL, the lance must be submerged in the slag, allowing the gas to be injected and dispersed directly within the liquid phase, this is the defining characteristic of the technology [14]. Conversely, TBRC technology involves blowing gas over the slag rather than injecting and dispersing it within, so the lance position must be optimized to fulfill its primary function of surface blowing [13].

3.5.3 Rotating wall speed

The TBRC technology is the only technology in metallurgical reactors that has a rotation system; the rotation speed causes the agitation and movement necessary for the transfer of energy and mass, as well as to promote chemical reactions by ensuring more uniform mixing within the molten bath [13].

3.5.4 Inclination angle

The inclination system is a specialized feature of the TBRC technology and has an effect both in the hydrodynamics and the physical reactor operation. When the reactor is inclined, the molten bath's exposure to the gas flow is adjusted, this enhances mixing and promote better mass and energy transfer. The reactor inclination system is also required to remove the molten material and the slag generated during the smelting process [12, 13, 20, 21].

3.6 Hydrodynamic insights from experimental and computational studies

The study of the hydrodynamics of bath smelting reactors has been a growing focus of attention in the scientific community and various authors have published on the effect of operational parameters on the hydrodynamic variables of both TSL and TBRC reactors, for example, Zhao *et al.* [23] through numerical simulations for a TSL reactor studied the effect of lance immersion depth on splashing and velocity patterns, finding a linear relationship between immersion depth and splashing. Additionally, their study highlights that at greater lance depths, "the circulating flow tended to move to the side wall."

The effect of lance penetration in TSL reactors was also studied by Obiso *et al.* [18] in 2019. In this study, through numerical simulations, they found that lance penetration into the slag increases the gas-liquid contact surface area, generates greater turbulence, and promotes more efficient mixing. A subsequent study by Obiso *et al.* [19] confirmed that higher lance positions leave significant portions of liquid near the bottom nearly stagnant, whereas deeper lance positions generate recirculating flows throughout the liquid volume. However, both authors mention the possibility that the turbulence caused by the deep positions of the lance could affect the matte sedimentation region at the bottom of the reactor, significantly reducing the reactor's efficiency.

The results of the aforementioned computational studies are consistent with the work of Akashi *et al.* [30], where in 2020 they designed a laboratory-scale model for an air-GaInSn TSL system. The physical properties of this mixture are very similar to the physical properties of industrial systems. The experiments confirmed that a higher gas flow produces more intense recirculation patterns and that the total area of the gas-liquid interface increases considerably when modifying the position of the lance together with the gas flow.

Operational parameters also affect the hydrodynamics in TBRC reactors. In 2020, Pérez-Tello *et al.* [20] studied through a scale cold-model how far the lance could penetrate before being contacted by slag droplets; a greater distance means less slag splashing. In this study, the effect of the rotation speed and the inclination of the reactor was evaluated. They found that higher rotational speeds slightly reduced lance penetration by increasing splashing, while vertical reactor positioning progressively increased splashing, preventing effective lance introduction even at an angle of 60° from the horizontal.

In 2024, Huang *et al.* [21] studied the effect of the same operational parameters on the mixing time using a scale model. Their findings demonstrated that increasing the reactor's rotational speed enhances turbulence and fluid mass transfer, reducing mixing time. They also identified an optimal inclination angle of 28°, which is typically used in real industry. However, they cautioned that excessive rotational speeds exacerbate the erosion of furnace bricks due to the ultra-strong turbulent vortex formed in the bath, thereby reducing reactor longevity.

These studies demonstrate that the operational parameters in TBRC and TSL reactors have a significant impact on hydrodynamics; however, there are no studies that integrate the fundamental characteristics of each technology into a single model. The objective of this work is to achieve that integration and study the effect of operational parameters on the system's hydrodynamics in a single TBRC-TSL model. For the study, only one parameter is changed while all others remain constant, thus isolating the modified parameter and analyzing the effect on the system's hydrodynamics. The following table (Table 3.4) summarizes the tested values for each operational parameter and in the next section, the results obtained from these simulations are presented.

Table 3.4: Operational parameters used for the simulations

Operational parameter	**Standard value**	**Values to be tested**	**Change (%)**
Mass flow rate ($\dot{m}$, kg/s)	2.152×10^{-5}	$1.076 \times 10^{-5}, 3.228 \times 10^{-5}$	$\pm 50\%$
Lance penetration depth (d/D)	0.867	$0.733, 0.8, 0.933$	$-15.4\%, -7.4\%, +7.6\%$
Rotation speed (ω, rpm)	95	$48, 143$	$\pm 50\%$
Inclination angle (θ, degrees)	45	$30, 60$	$\pm 33.33\%$

4 Results and discussion

4.1 Grid convergence study

The first study performed corresponds to the study of the computational mesh, this study is commonly performed in computational simulations to evaluate the accuracy of the mesh to be used. A finer mesh will always be more accurate than a coarser mesh but the computational cost will be much higher, the objective is to find a mesh that gives accurate results considering the computational resources available, a trade-off. For this study, 3 grids were created: A 330,000-cell grid (Figure 4.1 (a)), a 600,000-cell grid (Figure 4.1 (b)) and a 915,000-cell grid (Figure 4.1 (c)).

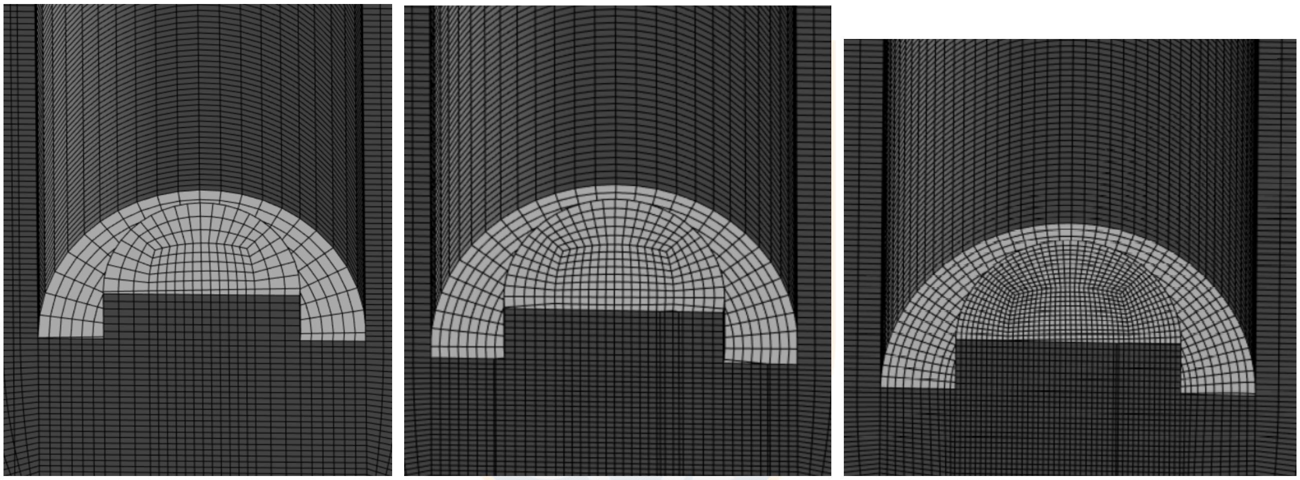

(a) 300,000 cell grid. (b) 600,000 cell grid. (c) 915,000 cell grid.

Figure 4.1: Computational meshes used for mesh study.

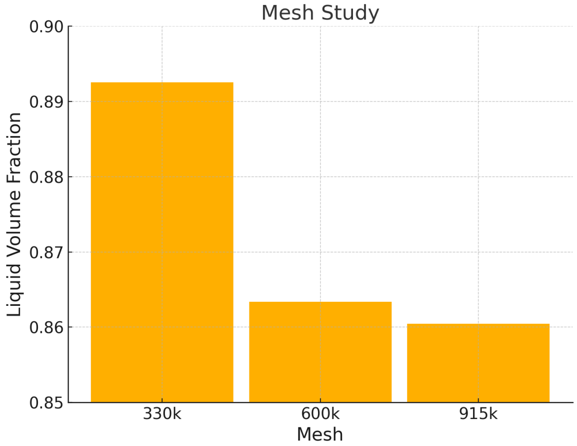

Figure 4.2: Liquid void fraction results for each grid.

The parameter to be evaluated corresponds to the liquid fraction in the zone that initially (before hydrogen injection) is filled with slag (liquid fraction = 1), this zone corresponds to the mustard-colored area in Figure 3.2 (b). Figure 4.2 shows the results obtained after weighting the values in the full time range. The results show an error of 3.73% between the coarsest grid and the finest grid and just of 0.34% between the 600,000 cell grid and the finest grid. The more refined computational mesh took three times the computational time of the coarsest mesh, while the 600,000 cell mesh took twice the time of the coarsest mesh. The coarsest mesh is able to process 0.01 seconds of simulation in 40 to 45 minutes of real time using 450 CPU's (High performance computing), therefore, considering the small error and the computational resources available the coarsest mesh is used for the simulations.

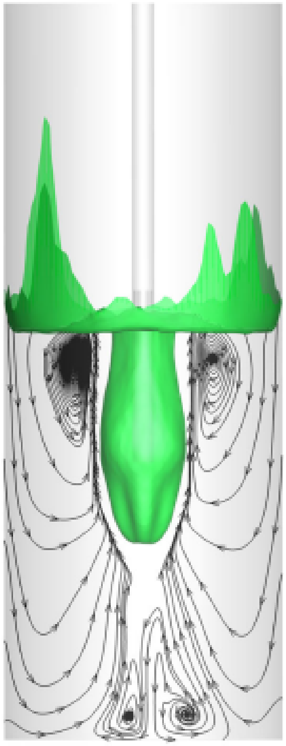

Figure 4.3: Recirculation phenomena. As bubbles rise liquid is sucked from the bottom. Adapted from [16].

4.2 Bubble Dynamics

Bath smelting reactors have a significant interaction between the liquid and gaseous phases, this interaction generates the appearance of bubbles which can vary in size, shape, speed, paths, etc. This transient behavior is known as bubble dynamics and has a significant effect on chemical reactions, mass transfer, and reactor efficiency. A bubble is defined as a spherical pocket of gas trapped within a continuum fluid, such as a liquid or partially molten solid [32]. Bubbles are generated at the gas injection point, where gas is dispersed into the metal bath or slag through a submerged lance. Thus, a gas-liquid interface is created.

4.2.1 Bubble Behavior and Recirculation Phenomena

As bubbles rise to the free surface due to buoyancy forces, they displace liquid upwards while simultaneously pushing the liquid at the free surface laterally. The depression in the wake of the bubbles sucks liquid metal from the bottom of the vessel upwards, leading to a recirculation phenomenon (Figure 4.5), this phenomenon, while promoting proper mixing, mass transfer, and reducing explosion risks, could also affect the sedimentation of metal at the bottom by overly stimulating the "slag-matte" layer, which would negatively impact the reactor's efficiency.

4.2.2 Effects of Bubble Frequency

A higher bubble frequency increases the liquid displaced, strengthening the recirculation effect. As more bubbles reach the surface, splashing occurs, which results from bubble breakup. As will be explained later, the bubbles and slag droplets are sources of gas-liquid interface, so an increase in the number of bubbles and droplets directly increases the total gas-liquid interface and then the mass transfer and chemical reactions.

4.2.3 Bubble Frequency Methodology

To determine the bubble frequency, a plane is set parallel to the plane containing the base of the reactor, both planes are separated by a distance of 0.05 m, the upper plane is used to monitor the gas fraction of the upward flow (Figure 4.4 (b)). The gas fraction is recorded every 0.01 seconds of simulation, which corresponds to a recording frequency of 100 Hz, sufficient to effectively capture the bubble frequency.

When bubbles pass through the monitoring plane, the time signal oscillates between 0 and 1: a value of 0 indicates that slag dominates the flow, while a value of 1 indicates no slag presence. Hence, values larger than 0 imply that the gas is passing through the plane, either as discrete bubbles or as a continuous stream. This behavior produces a periodic signal, as shown in Figure 4.4 (a).

The periodic signal in time is difficult to interpret and does not clearly provide information on frequency, repetitive patterns, or specific characteristics. To obtain the dominant frequency of each time signal a Fast Fourier Transform (FFT) is applied to the time signal. The FFT converts the signal from the time domain to the frequency domain, making it easier to identify the dominant frequency. Once FFT is applied to the time signal a frequency spectrum, reveals a distinct peak, however, to determine the bubble frequency, a signal smoothing is performed to eliminate the noise. Once the signal is smoothed, a Gaussian fit is performed, this is done because the FFT provides noise and secondary components that are not representative. The peak of the Gaussian fit smooths the signal, filters out the noise, and highlights the main frequency; then, the peak of the Gaussian fit is considered the bubble frequency (Figure 4.5).

4.2.4 Operational Parameters and Bubble Frequency

Using the method described above, the bubble frequency is determined for the different configurations studied (Table 3.4), the results are as follows:

- **Effect of gas flow rate** By increasing the gas flow by 50% the bubble frequency decreased from 8.84 to 8.24 Hz, which corresponds to a decrease of 6.8%. Conversely, by decreasing the gas flow by 50% the bubble frequency increased to 9.51 Hz, that is 7.5%. This behavior can be observed in Figure 4.6, the bubble frequency decreases with increasing gas flow.

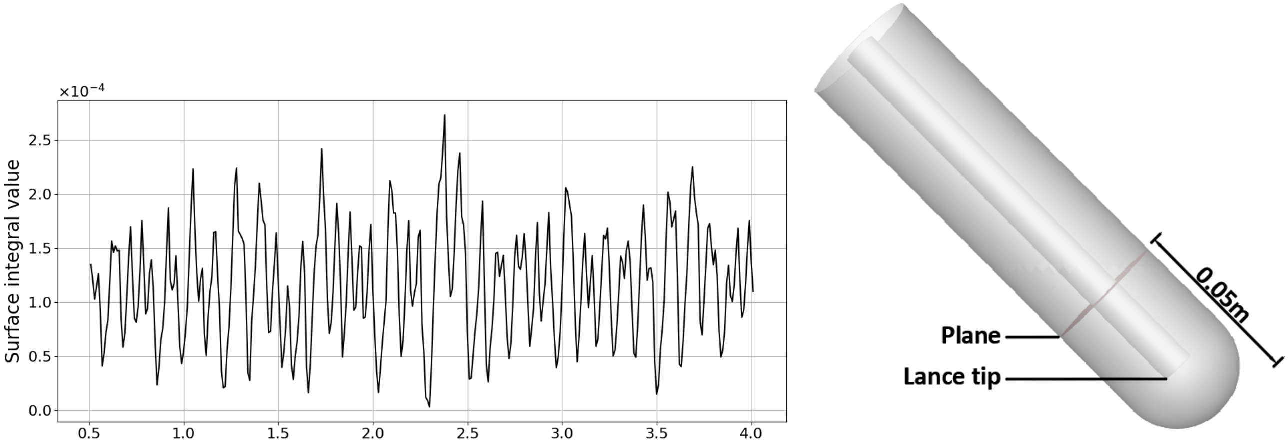

(a) The surface integral is tracked over time generating a periodic time signal.

(b) Monitoring plane to track the bubble frequency placed at Y=0.05m, above the lance tip.

Figure 4.4: Process for obtaining the periodic signal in time. A surface integral for the gas fraction is set up in the plane shown in (b), this signal is recorded every 0.01 seconds generating the time signal shown in (a). (a) Obtained time signal (b) Plane used for obtaining the signal.

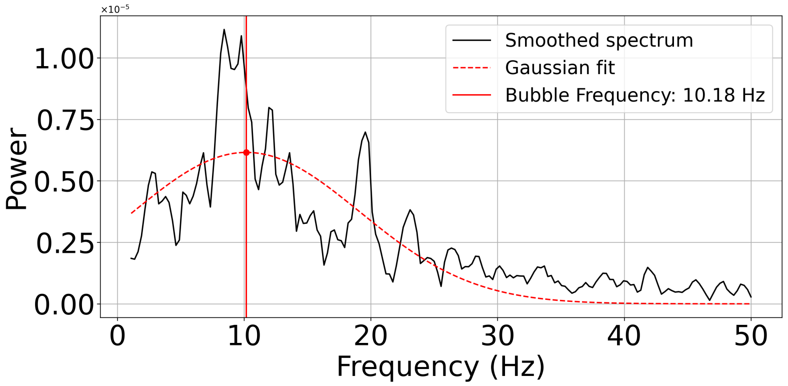

Figure 4.5: Once the time signal is obtained, an FFT is applied, which is then smoothed to eliminate noise, resulting in a smoothed spectrum shown with black curves. A Gaussian fit is then applied to the smoothed spectrum, corresponding to the red curve. The peak of the Gaussian fit is considered the bubble frequency.

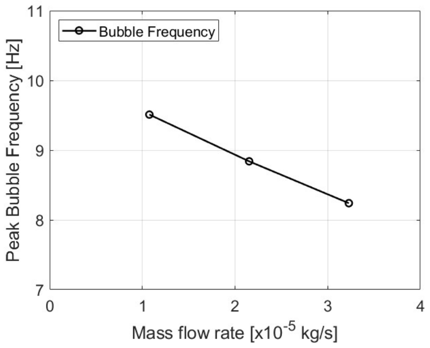

Figure 4.6: Peak Bubble Frequency plotted against mass flow rate.

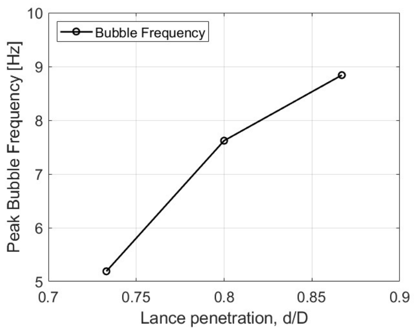

Figure 4.7: Peak Bubble Frequency plotted against lance penetration.

- **Effect of lance position** To determine the effect of the penetration of the lance, the dimensionless number d/D is used where D corresponds to the total length of the crucible and d corresponds to the length of the lance inside the crucible, taking the upper limit of the crucible as a reference, this dimensionless number determines the penetration of the lance in the crucible. It is important to note that the crucible has a wall thickness of 5 mm (Figure 3.2 (b)). The wall thickness does not influence the simulations since there is no heat gradient, so the wall is shown as a sheet and the crucible is raised 5 mm from the reference plane. This distance can be slightly appreciated in Figure 4.8. The effect of lance penetration on bubble frequency is shown in Figure 4.7, for this study d/D=0.933 was not considered due to data acquisition issues. By increasing the lance penetration from d/D=0.733 to d/D=0.867, i.e. by 18.3%, the bubble frequency increased from 5.10 to 8.83 Hz, this is an increase of 70%, evidencing the large impact of the lance penetration. These results are consistent with

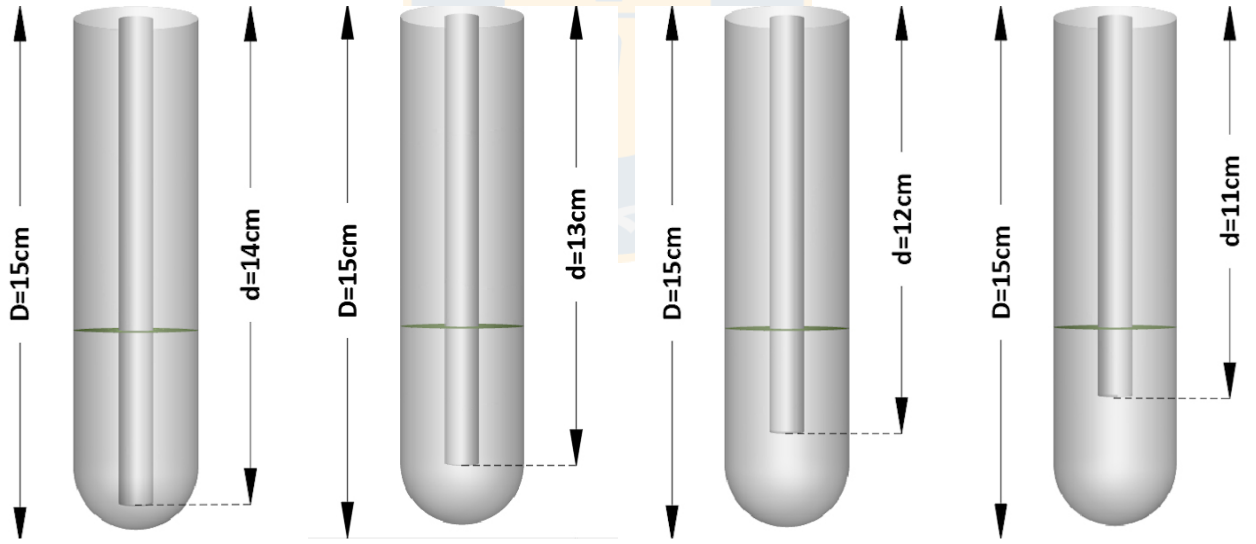

(a) d/D = 0.933 (b) d/D = 0.867 (c) d/D = 0.8 (d) d/D = 0.733

Figure 4.8: Diagram to represent the depth of the lance d/D. D corresponds to the total length of the crucible and d to the length of the lance taking the upper limit of the crucible as a reference.

those of Cao *et al.* [33] and Akashi *et al.* [30] where the bubble frequency also increased with increasing lance penetration, however, by 5 and 15%, respectively. The frequency range obtained in these 2 works was 12.5-19 Hz in the work of Cao *et al.* [33] and 10-14 Hz in the work of Akashi *et al.* [30] which is significantly higher than those obtained in this work (5.10 to 8.83 Hz). The main differences between this work and those mentioned above are: (1) The physical properties of the fluids (viscosity, surface tension and density) (2) The rotation and inclination of the vessel. Regarding the first one, the surface tension of the fluids in the work of Cao *et al.* [33] is 0.026 N/m, in the work of Akashi *et al.* [30] is 0.53 N/m and in this work is 0.55 N/m, the higher the surface tension, the lower the frequency range, this phenomenon has already been studied previously [34, 35]. Regarding the second, both the work of Cao *et al.* [33] and Akashi *et al.* [30] correspond to TSL configurations, i.e., without rotation and tilt, and as explained later, these parameters have a great impact on the bubble frequency. The obtaining of the bubble frequencies for each case can be seen from figures 9 to 11.

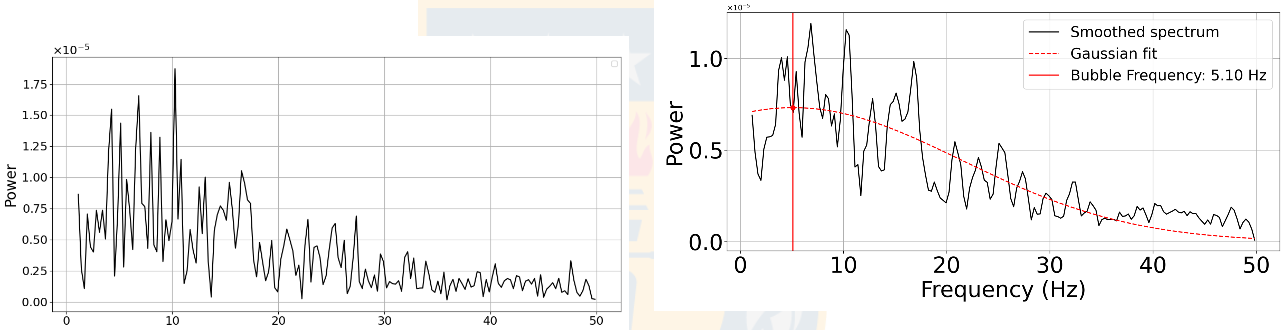

(a) Raw FFT.

(b) Smoothed spectrum, Gaussian fit and Peak Bubble Frequency.

Figure 4.9: Lance penetration: 0.733. Peak Bubble Frequency 5.10 Hz.

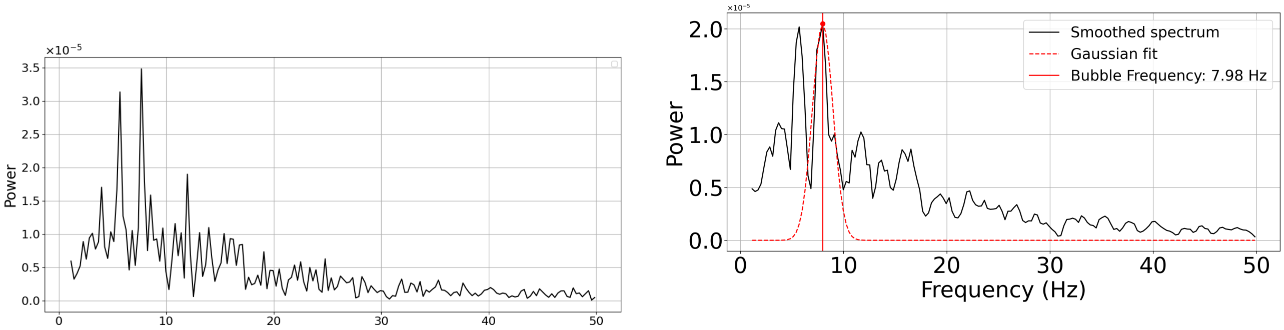

(a) Raw FFT.

(b) Smoothed spectrum, Gaussian fit and Peak Bubble Frequency.

Figure 4.10: Lance penetration: 0.8. Peak Bubble Frequency 7.98 Hz.

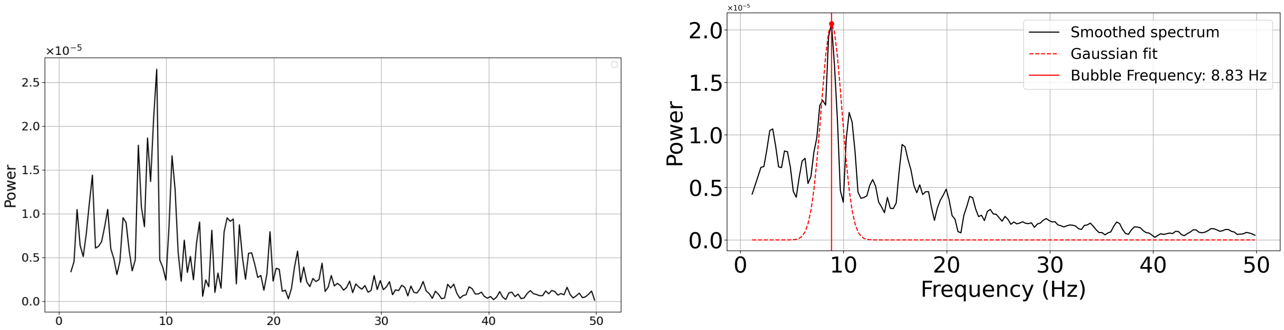

(a) Raw FFT.

(b) Smoothed spectrum, Gaussian fit and Peak Bubble Frequency.

Figure 4.11: Lance penetration: 0.867. Peak Bubble Frequency 8.83 Hz.

- **Effect of inclination** The effect of the tilt is shown in Figure 4.12. By increasing the inclination angle from 30 to 60 degrees, i.e., doubling the tilt, the bubble frequency increased from 6.61 to 9.98 Hz, which is a significant 51% increase. As explained in the previous paragraph, this effect could also be a cause of the large decrease in the frequency range obtained in this work compared to the frequency ranges obtained in the work of Cao *et al.* [33] and Akashi *et al.* [30] where the vessel was completely vertical.
- **Effect of rotation speed** The effect of rotational speed can be seen in Figure 4.13. The bubble frequency tends to decrease noticeably with increasing rotational speed. The graph shows a 19.6% decrease in bubble frequency with a tripling of the rotational speed. It is interesting to note that the lower the rotational speed the more pronounced the change in bubble frequency. This result is consistent with the decrease in the frequency range between this study and that of Cao *et al.* [33] and Akashi *et al.* [30] that was explained in the last 2 paragraphs.

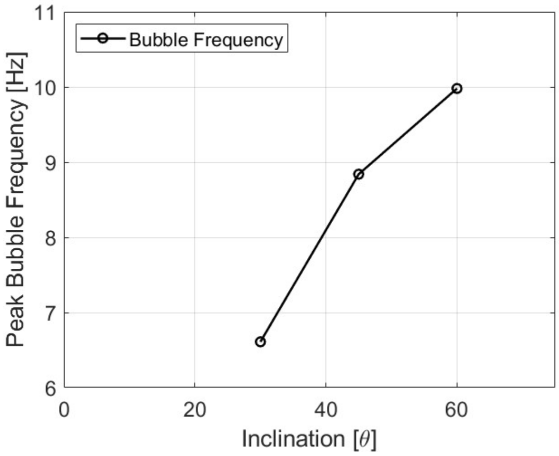

Figure 4.12: Peak Bubble Frequency plotted against inclination. The angle is measured based on the horizontal axis.

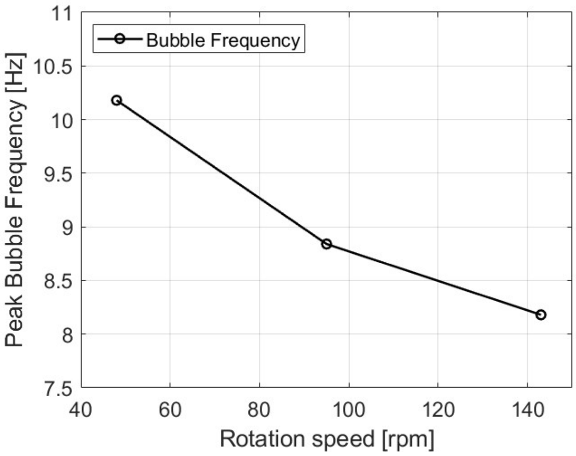

Figure 4.13: Peak Bubble Frequency plotted against rotation speed.

4.3 Slag Splashing

Slag splashing is a fundamental phenomenon in the hydrodynamics of a TSL and TBRC reactor. Slag splashing corresponds to the aggressive displacement of slag droplets throughout the reactor. Slag droplets are a source of liquid-gas interface, therefore a larger amount of slag droplets, or a more intense splashing increases the total surface of the liquid-gas interface, this interface leads the smelting process. This sequence of events gives a unique feature to TSL reactors since they can rapidly control the mass transfer surface. However, intense splashing causes slag droplets to be in constant contact with the reactor walls and even the reactor roof, as well as with the reactor central lance.

The first case causes increased wear on the reactor walls due to mechanical erosion, chemical corrosion and thermal cycling and the second case is beneficial since the slag solidifies on the lance surface creating a protective layer that preserves the lance from the aggressive environment and from a direct contact with the slag and therefore it prolongs the lifetime of the lance [14, 18]. The solidification of the slag occurs due to the cold gas circulating inside the lance.

The numerical simulations track the maximum height reached by slag droplets at each time step. This is achieved by using the Volume of Fluid (VOF) method in ANSYS Fluent, which accurately captures the gas-liquid interface of the slag droplets.

ANSYS Fluent identifies the cell farthest from the crucible base that belongs to this interface. It then calculates the perpendicular distance from the plane at the crucible base to this cell. This distance represents the maximum height of the slag at that specific moment.

The height ranges from 0 (at the base of the crucible) to 0.15 m (at the top of the crucible). A visual representation of this method is provided in Figure 4.14.

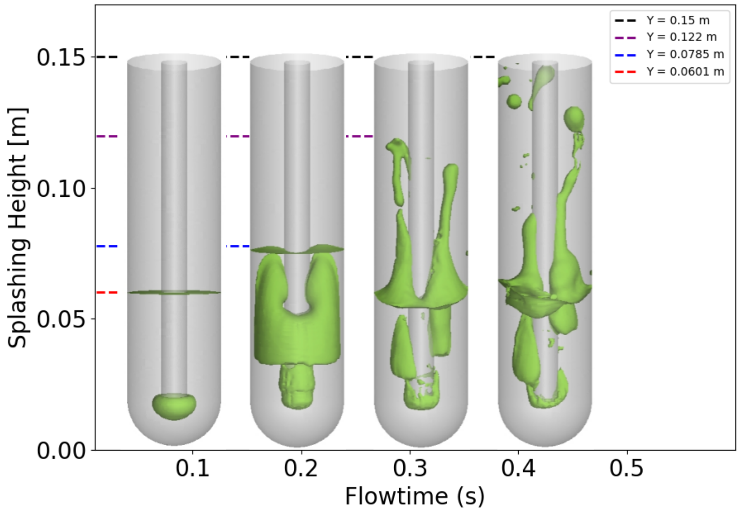

Figure 4.14: Splashing height plotted against flowtime. The farthest distance to the base of the crucible where there is an interface will be considered the maximum splashing height.

- **Effect of gas flow rate** Figure 4.15 shows the results for the effect of gas flow on splashing height, with an increase in gas flow of 50% the mean splashing height increased by 6.1% while decreasing gas flow by 50% the mean splashing height decreased by 9%. For the flow range from 1.076-3.228 x 10^{-5} kg/s the mean splashing height remained between 0.1234 and 0.1407 m. The splashing height is directly proportional to the gas flow rate.
- **Effect of lance position** The effect of lance penetration is visualized in Figure 4.16. The trend is clear, as the lance penetrates the crucible the mean splashing height increases considerably, from a penetration of 0.733 to 0.867 the mean splashing height increased from 0.101 to 0.132 m, this is an increase of 30.7%. In this range the lance penetration is the most influential parameter on the splashing height, however, in the penetration range from 0.867 to 0.933 a decrease in the average splashing height is observed, probably due to the extreme closeness to the bottom of the crucible.
- **Effect of inclination** The effect of the crucible's inclination is seen in Figure 4.17. While the trend is not as clear as for lance penetration, the splashing height increases steadily with inclination angle, in fact, by doubling the inclination angle (From 30 to 60 degrees), the mean splashing height increased by 11%. This trend is consistent with the study of Pérez-Tello *et al.* [20] where for an inclination range of 30 to 60 degrees the splashing steadily increased and even for an angle of 60 degrees the splashing was able to touch the upper limit of the vessel.
- **Effect of rotation** The effect of rotation can be seen in Figure 4.18. increasing the rotational speed from 48 to 95 rpm produces a decrease in the mean splashing height; however, further increasing the rotational speed causes the mean height to increase again. Increasing the rotational speed from 95 to 143 rpm, that is an increase of 50%, produces an increase in the mean splashing height of 4.8% while decreasing the rotational speed by 50% (From 95 to 48 rpm) increased the mean splashing height by 5.6%. Then, rotational speed plays a minority role in the splashing height for the range of 48 to 143 rpm. This result is also consistent with the work presented by Pérez-Tello *et al.* [20].

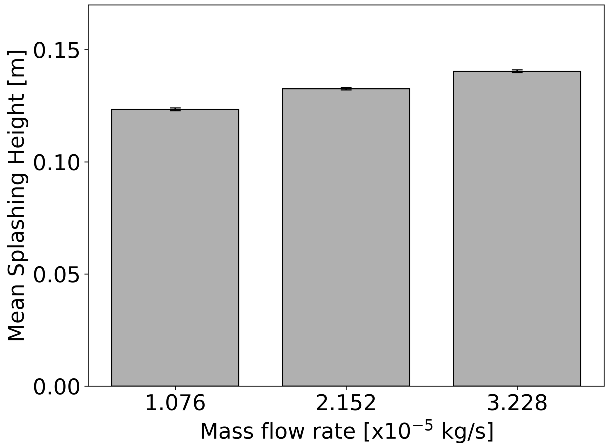

Figure 4.15: Splashing height plotted against mass flow rate. *Error bars were calculated as the standard error of the mean.*

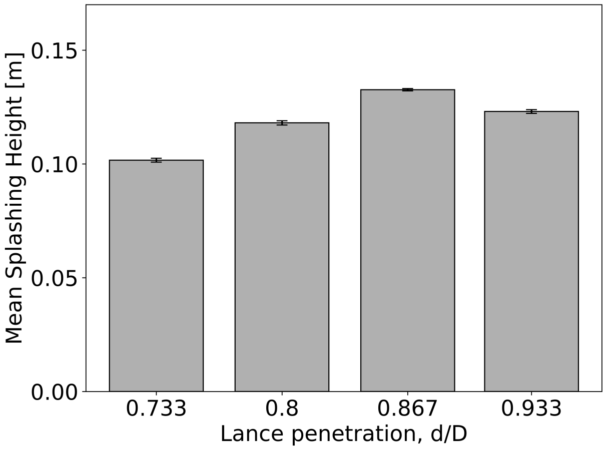

Figure 4.16: Splashing height plotted against lance penetration. *Error bars were calculated as the standard error of the mean.*

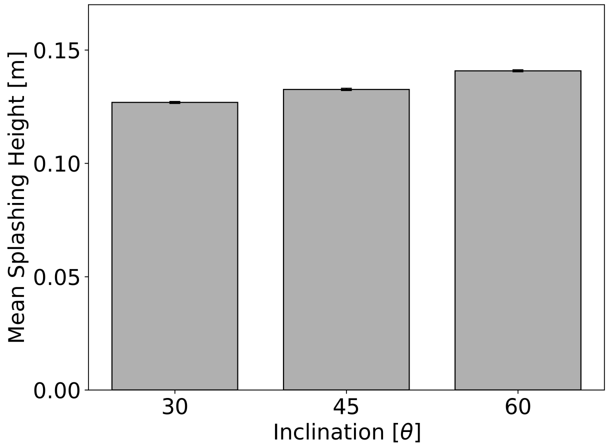

Figure 4.17: Splashing height plotted against inclination. *Error bars were calculated as the standard error of the mean.*

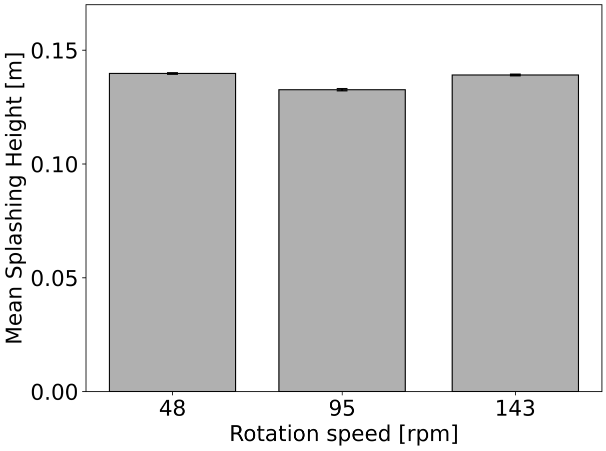

Figure 4.18: Splashing height plotted against rotation speed. *Error bars were calculated as the standard error of the mean.*

4.4 Slag-gas Interface Area

The mechanism by which the gas is introduced is different between TBRC and TSL reactor technology. In TSL reactors, the gas is introduced directly into the bath, whereas in TBRC reactors, it is blown over the bath. This operational difference has a profound impact on the slag-gas interface area. Because in the computational model created and used in this work, the lance is always submerged in the molten bath, the slag-gas interface is analyzed from the a TSL technology standpoint.

The slag-gas interface represents the area where the gas phase directly interacts with the slag phase, in this area, mass transfer and chemical reactions occur. In TSL reactors, this interface is produced from different sources: the surface of the primary bubble at the tip of the lance, the entrainment of gas within the bath, the free surface of the bath, and the droplets of liquid slag splashed into the gas phase [16] (Figure 4.19). These components are highly dynamic, with their total surface area fluctuating continuously in space and time due to chaotic flow, fluid properties, and operational conditions. The unpredictable behavior and the constant movement of the interface make direct measurement very difficult, specially in industrial reactors where temperatures exceed 1300 K and toxic gases are often involved. For this reason, estimates of the total interface area are usually based on the bubble frequency and the reaction conversion rates [16].

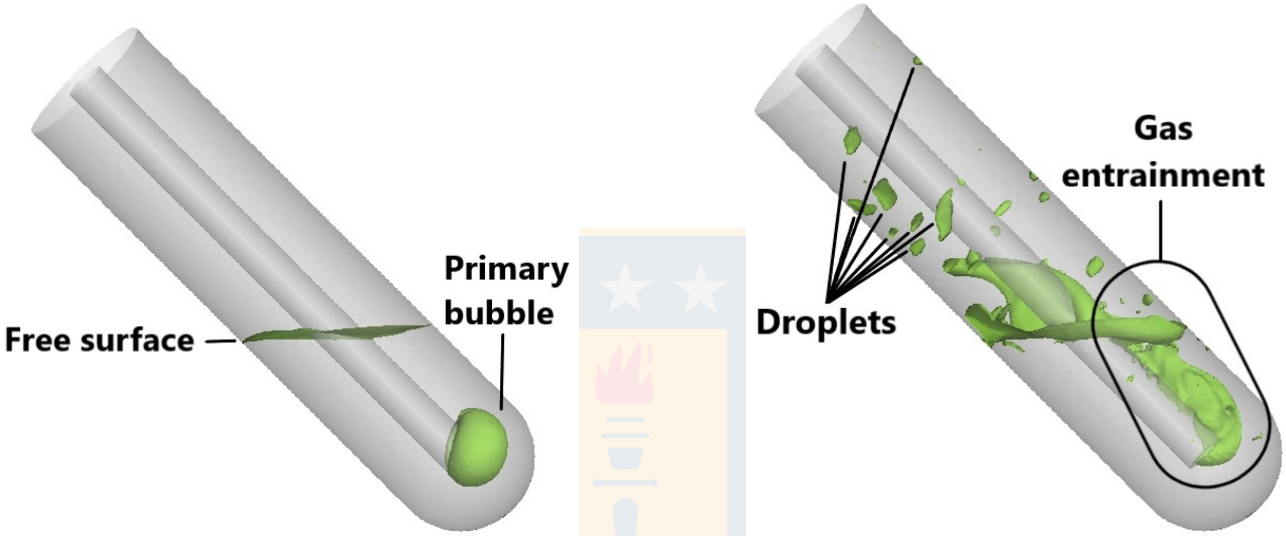

(a) Primary bubble forms at the tip of the lance and the free surface separates the slag and gas phases.

(b) The gas passes through the slag in the form of small bubbles or streams. Once it reaches the free surface, splashing occurs and the slag forms droplets that jump violently through the gas phase.

Figure 4.19: Gas-liquid interface sources. The interface is displayed in green.

To track the interface behavior, simulations are a powerful alternative. Obiso *et al.* [18] demonstrated the accuracy of numerical models by comparing experimental results with CFD simulations, highlighting their capability to predict complex phenomena with high precision.

In this study, Ansys Fluent was used to track the slag-gas interface in both space and time, providing total interface area values at each time step. The goal is to evaluate the changes on the total interface area for different operational conditions. Simulations were conducted over a period of 4 seconds of flow time, with the initial 0.5 second excluded to allow the system to stabilize from its inertial state.

- **Effect of gas flow**

  The first operational parameter modified is the gas flow rate which was increased and decreased by 50%. The results show a proportional increase between the interface area and the gas flow rate (Figure 4.20). As the gas flow increased by 50% the interface increased by 25% and as the flow decreased by 50% the interface decreased by 24%. These values indicate that there is a nearly linear proportionality between gas flow and interface area. With the aim of deepening the sensitivity of the interface to gas flow, the sensitivity coefficient is calculated. This is a measure that describes how the variation of an input parameter (in this case, gas flow) affects an output variable (Interface area). When calculating the sensitivity coefficient (S) using the formula:

$$S = \frac{\Delta(\text{Interface})}{\Delta(\text{Mass flow rate})} \tag{4.1}$$

Is obtained:

Decreased flow by 50%

$$\begin{aligned}
\Delta(\text{Interface area}) &= (3.48841 \times 10^{-3}) - (2.65231 \times 10^{-3}) = 0.8361 \times 10^{-3} \\
\Delta(\text{Mass flow rate}) &= -50\% = -0.5 \\
S_{\text{decrease}} &= \frac{0.8361 \times 10^{-3}}{-0.5} = -1.6722 \times 10^{-3}
\end{aligned}$$

Increased flow by 50%

$$\begin{aligned}
\Delta(\text{Interface area}) &= (4.37644 \times 10^{-3}) - (3.48841 \times 10^{-3}) = 0.88803 \times 10^{-3} \\
\Delta(\text{Mass flow rate}) &= +50\% = +0.5 \\
S_{\text{increase}} &= \frac{0.88803 \times 10^{-3}}{0.5} = 1.7761 \times 10^{-3}
\end{aligned}$$

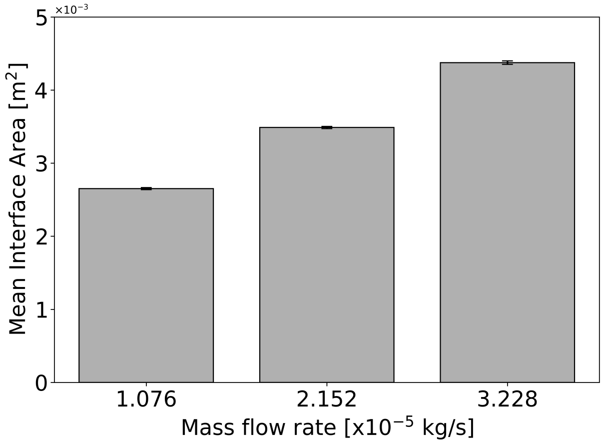

Figure 4.20: Interface area plotted against mass flow rate. *Error bars were calculated as the standard error of the mean.*

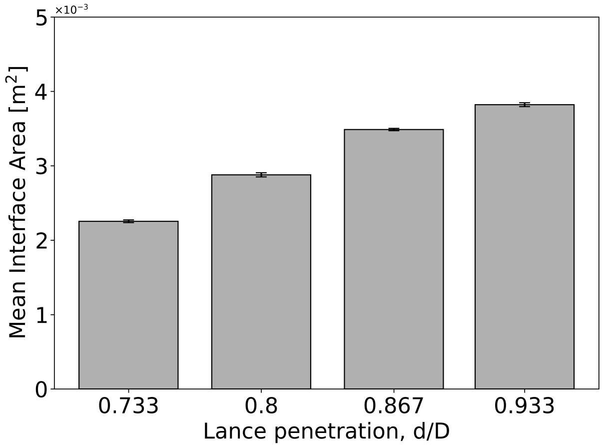

Figure 4.21: Interface area plotted against lance penetration. *Error bars were calculated as the standard error of the mean.*

These coefficients show that the interface is moderately sensitive to changes in gas flow. The slight difference between the values as the flow rate increases and decreases means there is nonlinearity in the behavior of the system.

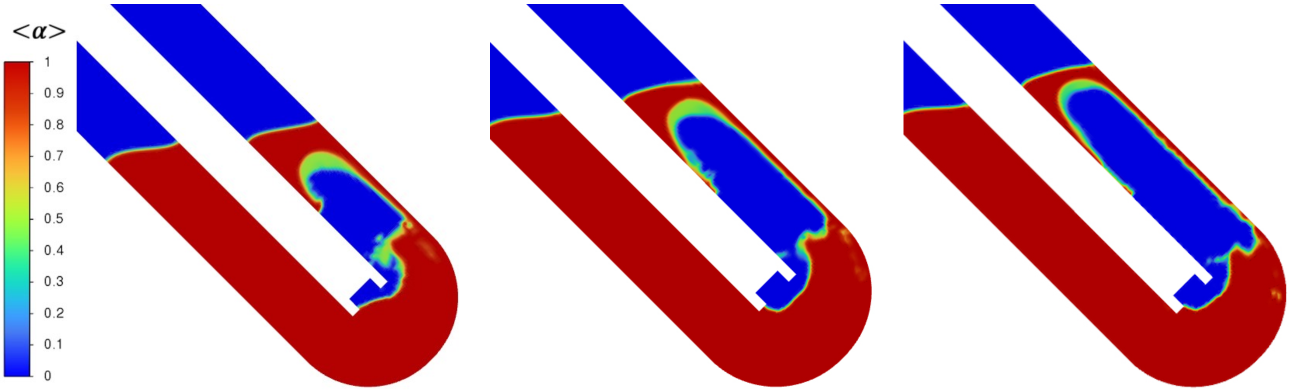

(a) Gas flow rate decreased by 50%. (b) Original gas flow rate. (c) Gas flow rate increased by 50%.

Figure 4.22: Liquid void fraction snapshots at the same flowtime for the three gas flow rate cases. The primary bubble becomes larger as the gas flow rate increases.

Figure 4.22 shows the sensitivity of the total interface area to gas flow rate. It is observed that with increasing gas flow rate both the primary bubble and the gas entrainment are significantly larger which directly causes an increase in the total area of the interface.

- **Effect of lance position.**

  The increase in total interface area as the lance penetration increases is noticeable (Figure 4.21). In the range from d/D=0.733 to d/D=0.933 the total interface area increased by 70%. As the lance penetrates further into the slag there is a greater amount of gas passing through the slag and hence a greater amount of bubbles coexist, furthermore, the results in section 4.3. show an increase in splashing up to a certain depth of the lance. All of these factors directly impact the total interface area. These results are consistent with the study of Obiso *et al.* [18].

- **Effect of inclination** Figure 4.24 shows a direct dependence between the total interface area and the crucible inclination. By increasing the crucible inclination by 15 degrees (From 45 to 60 degrees, +33.33%) the total interface area increased by 4.2% while decreasing the crucible inclination by 15 degrees (From 45 to 30 degrees, -33.33%) the total interface area decreased by 9.3%. The 90 degrees configuration corresponds to the TSL technology, by increasing the reactor inclination from 30 to 90 degrees, i.e., tripling the inclination, the total interface area increases by 31%. The increase in the total interface area is due to 2 main causes: (1) The bubble rise path from the tip of the lance to the free surface is longer as the angle increases, this generates more contact time between the liquid phase and the gas phase, therefore, the gas entrainment through the slag is larger (Figure 4.23). (2) As the angle increases so does the maximum height of the slag droplets, the droplets are suspended in the gas phase for a greater amount of time, increasing the gas-liquid interaction (Figure 4.17).

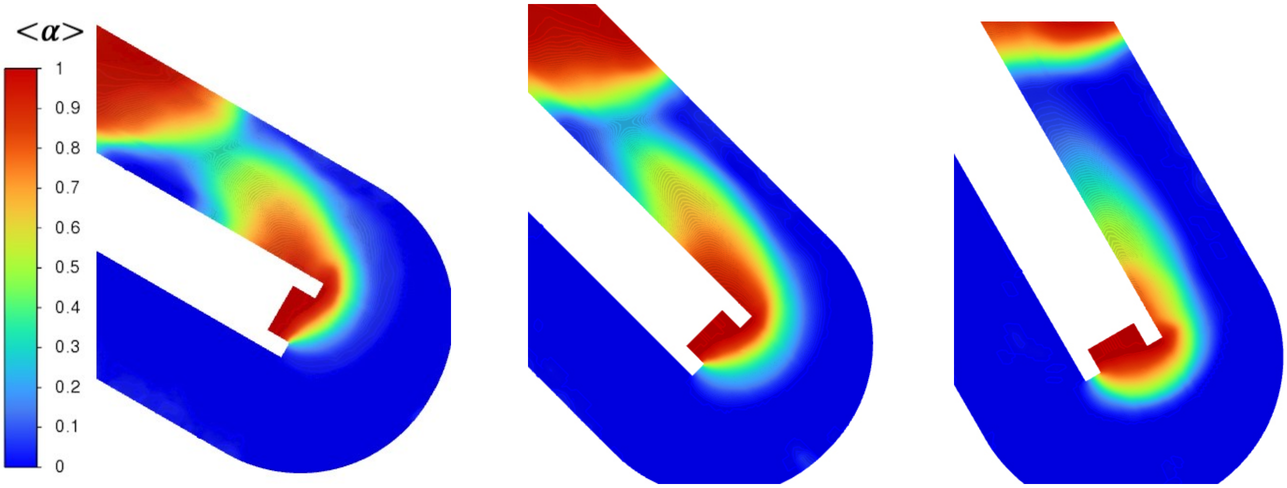

(a) θ=30 degrees. (b) θ=45 degrees. (c) θ=60 degrees.

Figure 4.23: Time-averaged gas void fraction. The red zone can be interpreted as the probability of finding gas.

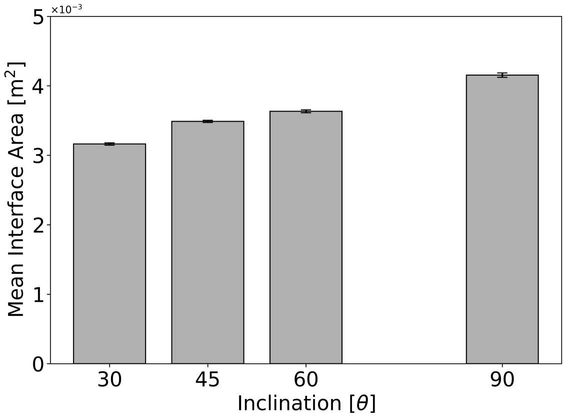

Figure 4.24: Interface area plotted against inclination. *Error bars were calculated as the standard error of the mean.*

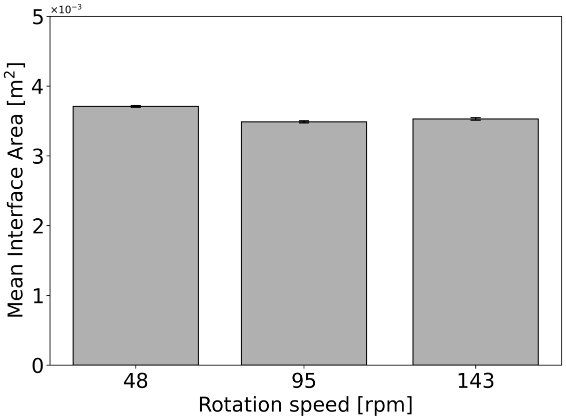

Figure 4.25: Interface area plotted against rotation speed. *Error bars were calculated as the standard error of the mean.*

- **Effect of rotation speed**

The effect of rotation speed can be seen in Figure 4.25. By decreasing the rotation speed by 50% the total interface area increased by 5.9% while increasing the rotation speed by 50% the effect is negligible. Figure 4.26 shows the time-averaged gas fraction, the red area can be interpreted as "the probability of encountering gas", it is noted that as the rotation speed increases, the probability of encountering gas through the slag decreases, as fewer bubbles pass through the slag the total gas-liquid interface decreases (Bubbles through the slag are a source of gas-liquid interface). In addition, it is interesting to note that as the crucible rotation increases, the magnitude of fluid velocity decreases in the middle zone of the crucible and increases near the walls as shown in Figure 4.27, this phenomenon is dominated by the centrifugal force that is generated by the rotation of the crucible.

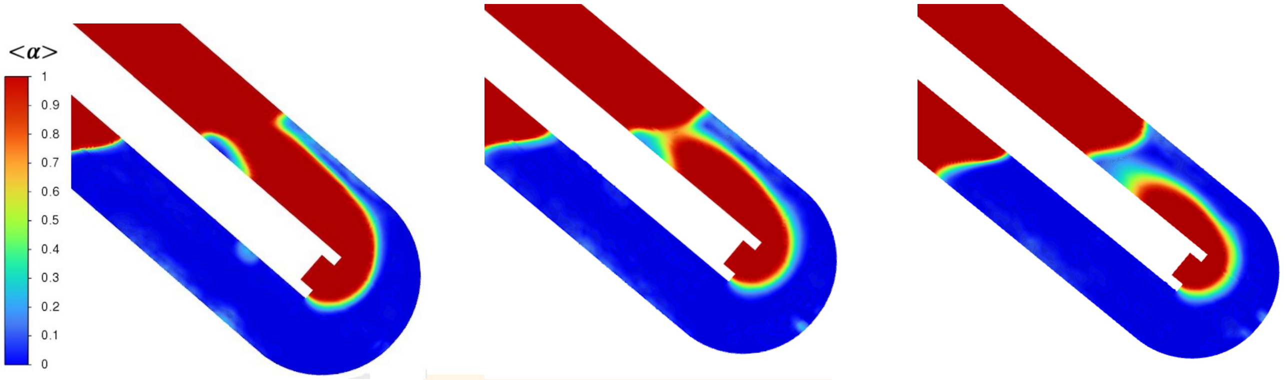

(a) Rotation speed: 48 rpm.

(b) Rotation speed: 95 rpm.

(c) Rotation speed: 143 rpm.

Figure 4.26: Time-averaged gas void fraction for rotation speeds of (a) 48 rpm (b) 95 rpm and (c) 143 rpm The red zone can be interpreted as the probability of finding gas.

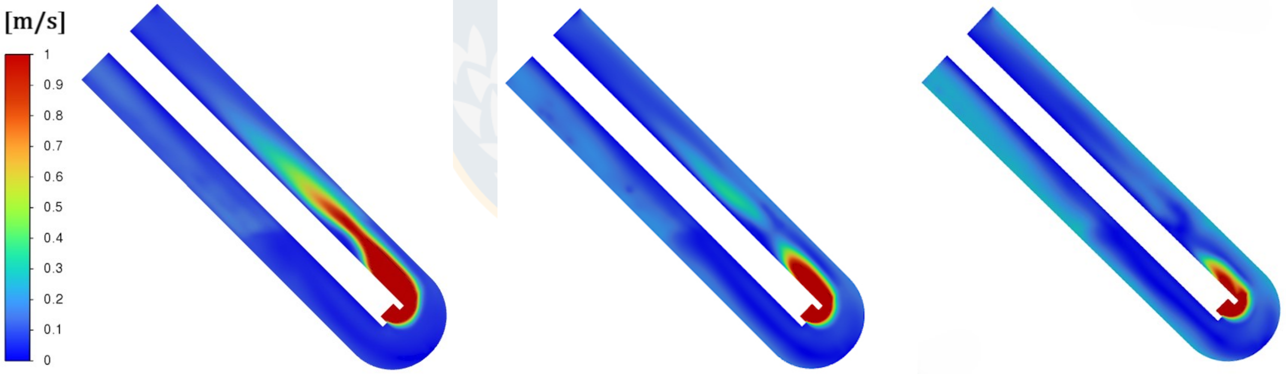

(a) Rotation speed: 48 rpm.

(b) Rotation speed: 95 rpm.

(c) Rotation speed: 143 rpm.

Figure 4.27: Mean velocity magnitude for rotation speed of (a) 48 rpm (b) 95 rpm and (c) 143 rpm. As the rotation speed increases the velocity magnitude shifts towards the crucible wall.

4.5 Velocity distribution and flow patterns

The main characteristic of TSL technology is the gas injection mechanism, which consists in the gas injected directly into the smelting bath, causing significant hydrodynamic effects such as agitation, turbulence, and recirculation zones. These effects enhance mass transfer, heat transfer, the rate of chemical reactions and even are safety related. However, excessive agitation and turbulence are not always beneficial.

In TSL technology, the matte typically sediments to the bottom of the reactor by gravity. Excessive turbulence can disturb this sediment layer, reducing process efficiency. Furthermore, strong agitation and turbulence can accelerate wear on the lance and refractory lining, leading to increased maintenance requirements and more frequent shutdowns.

Now then, in the case of low agitation and turbulence, it could result in areas of stagnation or poor recirculation. These areas not only decrease reaction rates but can also lead to the accumulation of solids. If these solids contain uncombusted fuel, they pose a significant safety risk, potentially causing explosions [18].

Consequently, the velocity distribution and flow patterns are critical hydrodynamic parameters that significantly influence reaction efficiency, equipment wear, and process safety, underscoring the need for a thorough understanding of these factors.

Several studies have established links between operational parameters and the velocity distribution and flow patterns in TSL and TBRC reactors [18, 20, 21, 23]. Using the post-processing tools available in ANSYS Fluent, the impact of different operational parameters can be analyze by generating time-averaged velocity contours and streamlines, as well as instantaneous snapshots at specific time. The tools provided by Ansys FLUENT are extensively used in hydrodynamics studies and are highly accurate.

- **Effect of gas flow**

  The first operational parameter modified is the gas flow rate which was increased and decreased by 50%. As the gas flow varies the axial and radial velocities of the fluids inside the reactor change drastically. Both components are directly proportional to the gas flow, in Figure 4.28 is shown the time-averaged axial velocity, as the inlet flow increases the gas rises with more force and there is a greater amount of both slag and gas moving in the positive direction of the axial axis. The time-averaged radial velocity is shown in Figure 4.29, as mentioned above, this component also increases directly with gas flow. As the gas rises with greater force it generates a greater suction of the liquid from the bottom which then flows down the reactor walls, this phenomenon is called recirculation and can be seen in Figure 4.30, the greater the amount of gas entering the crucible the more pronounced the recirculation, especially in the lower part of the crucible.

- **Effect of lance position** The position of the lance has a great impact on the recirculation phenomenon. Contrary to expectations, the higher the position of the lance, the better the recirculation in the lower part of the crucible. On the one hand, Figure 4.31 shows the axial component of the time-averaged velocity, the streamlines show how as the lance approaches the base of the crucible the recirculation vortices become weaker, in image 4.31 (d) there is no recirculation vortex at the bottom. On the other hand, Figure 4.32 shows the radial component of the time-averaged velocity for a plane located close to the base of the crucible, in this area it can be clearly seen that the recirculation vortices become weaker also as the lance increases its depth, in fact, for the position of the lance d/D=0.933 there is no clear recirculation vortex in the lower part of the plane, this area corresponds to the deepest part of the crucible.

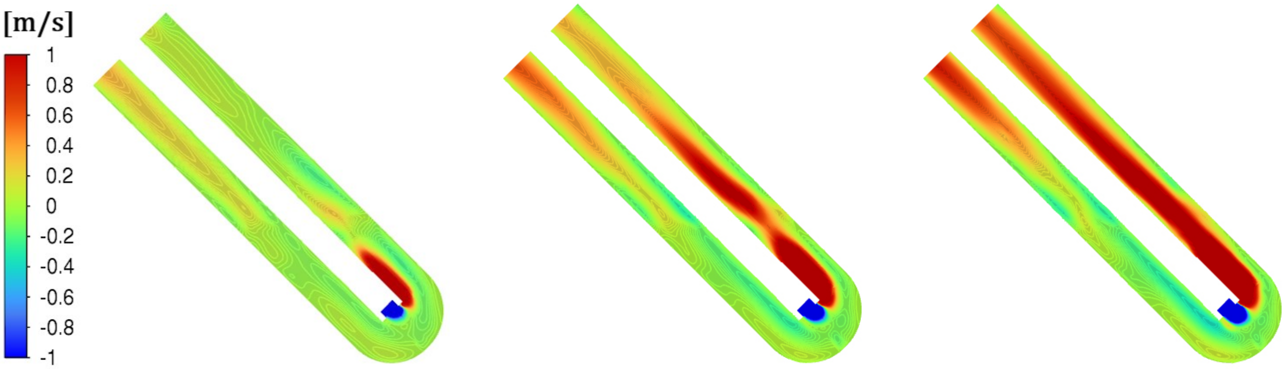

(a) Gas flow rate: 1.076 x [10^{-5} kg/s] (b) Gas flow rate: 2.152 x [10^{-5} kg/s] (c) Gas flow rate: 3.228 x [10^{-5} kg/s]

Figure 4.28: Time-averaged axial velocity.

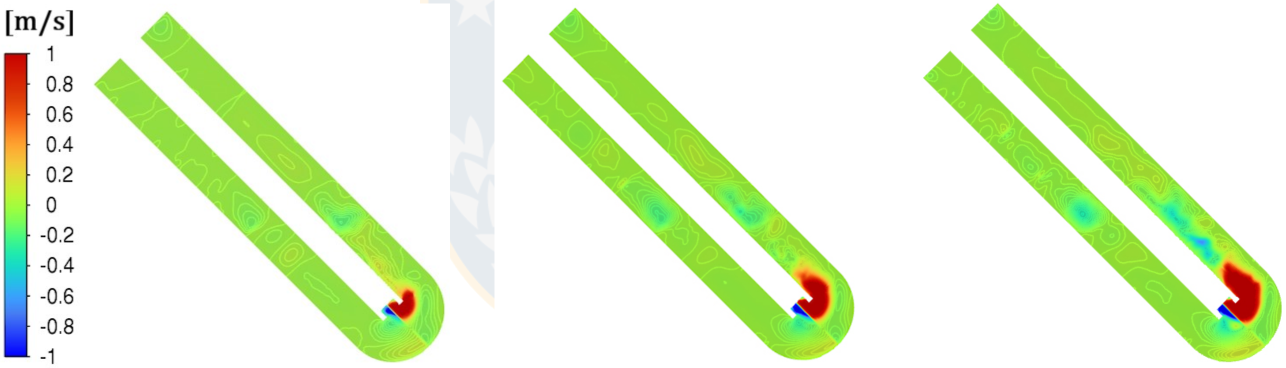

(a) Gas flow rate: 1.076 x [10^{-5} kg/s] (b) Gas flow rate: 2.152 x [10^{-5} kg/s] (c) Gas flow rate: 3.228 x [10^{-5} kg/s]

Figure 4.29: Time-averaged radial velocity.

- **Effect of rotation speed**

Rotation has a great impact on the axial and radial velocities of the fluids. This effect can be clearly seen in Figure 4.27 where, as the rotation speed increases, the velocity along the wall increases. On the contrary, as the rotation speed decreases, the gas concentrates in the inner zone of the crucible, near the lance (Figure 4.26), then, the gas rises rapidly and at a higher velocity (Figure 4.33). The radial flow patterns can be seen in Figure 4.34, as in the previous case, these images correspond to the time-averaged radial velocity for a plane at the bottom of the crucible, in Figure 4. 34 (a) there is a third vortex which as the rotation speed increases merges with the lower vortex, generating a larger vortex, this means that the radial

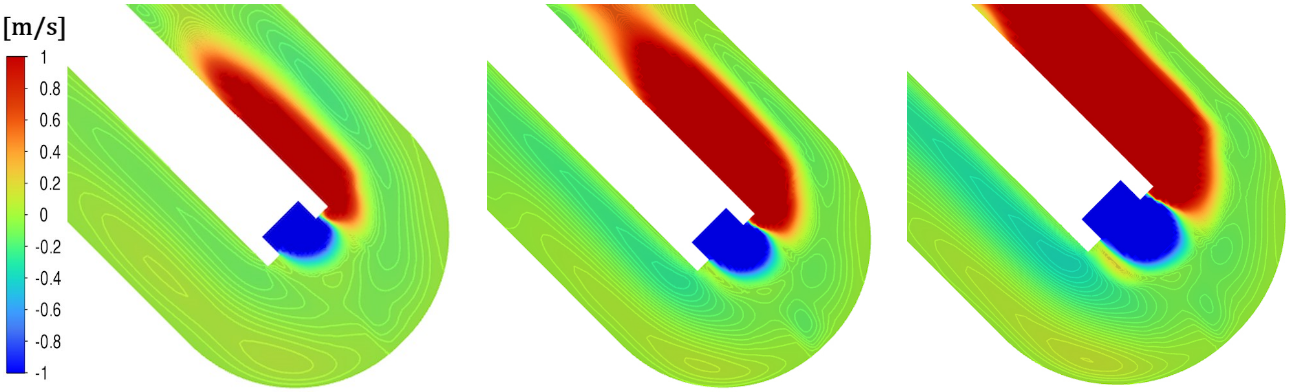

(a) Gas flow rate: 1.076 x [10^{-5} kg/s] (b) Gas flow rate: 2.152 x [10^{-5} kg/s] (c) Gas flow rate: 3.228 x [10^{-5} kg/s]

Figure 4.30: Time-averaged axial velocity. The streamlines show the recirculation phenomena, as the gas flow rate increases the recirculation phenomena is stronger.

recirculation in the lower part of the reactor is greater as the rotation increases, this result is consistent with Figure 4.27 (c) where a greater magnitude of velocity is observed in the lower part of the wall.

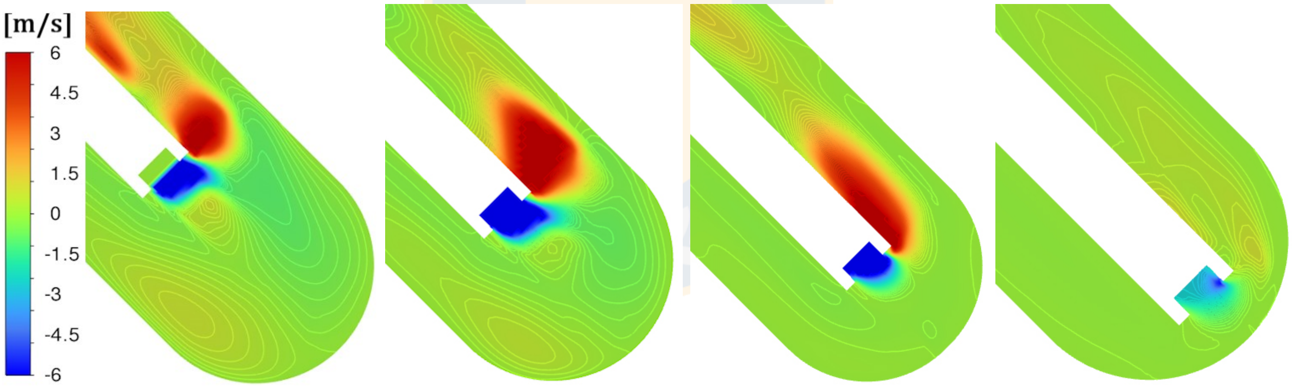

(a) d/D=0.733 (b) d/D=0.8 (c) d/D=0.867 (d) d/D=0.933

Figure 4.31: Time-averaged axial velocity.

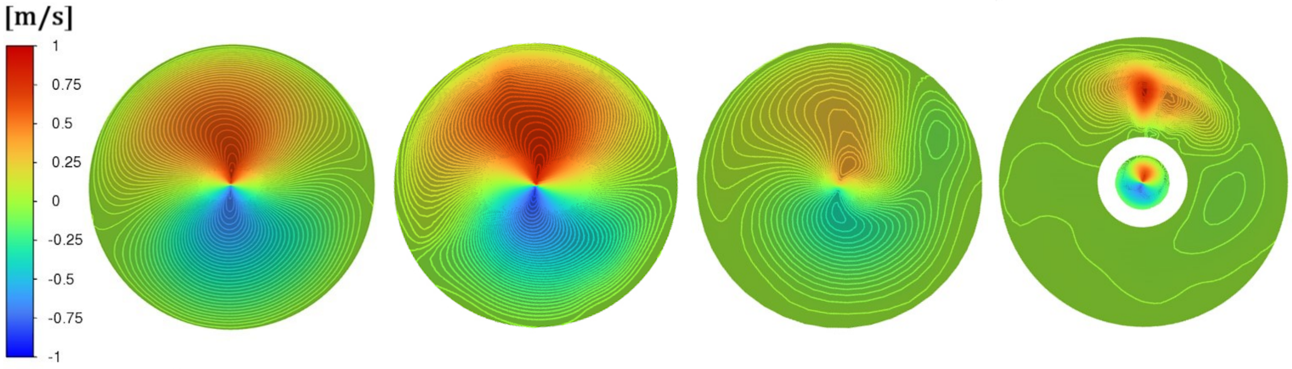

(a) d/D=0.733 (b) d/D=0.8 (c) d/D=0.867 (d) d/D=0.933

Figure 4.32: Time-averaged radial velocity. The plane is set at Y=0.012m.

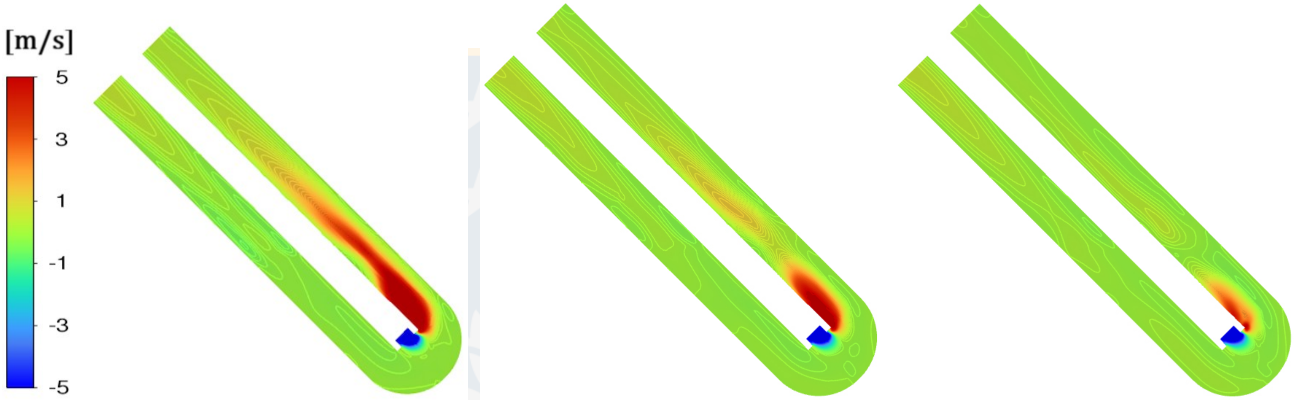

(a) Rotation speed: 48 rpm. (b) Rotation speed: 95 rpm. (c) Rotation speed: 143 rpm.

Figure 4.33: Time-averaged axial velocity. As the rotation speed increases the gas raises with a higher velocity through the crucible.

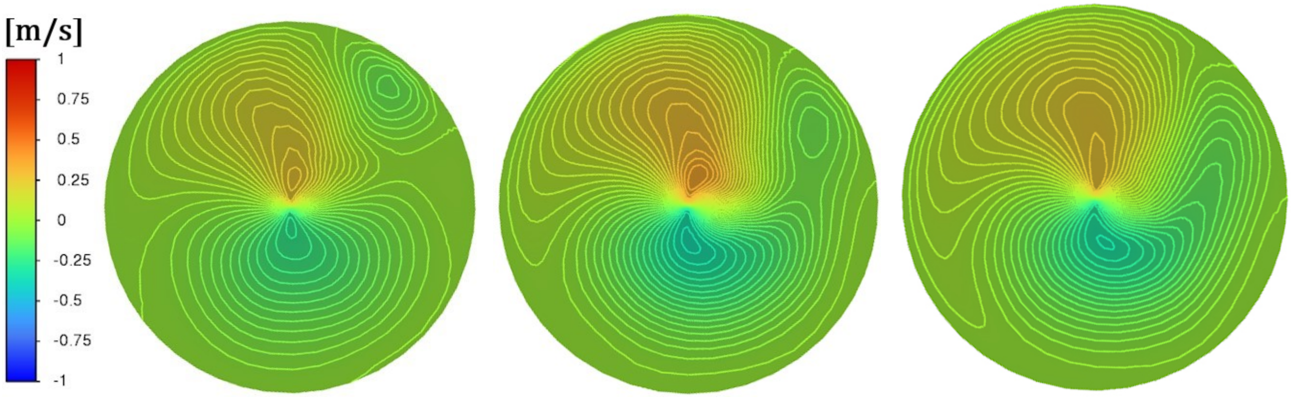

(a) Rotation speed: 48 rpm. (b) Rotation speed: 95 rpm. (c) Rotation speed: 143 rpm.

Figure 4.34: Time-averaged radial velocity. The radial recirculation phenomena gets stronger as the rotation speed increases.

- **Effect of inclination**

  The inclination of the reactor does not show effects as noticeable as the position of the lance or the gas flow, however, in Figure 4.35 it can be seen how the axial velocity tends to decrease in the bubble rising zone as the crucible inclination increases. The axial recirculation zones in the lower part of the crucible remain practically unchanged. The radial flow patterns change slightly, in Figure 4.36 it can be seen that as the inclination increases the recirculation becomes less intense, this can be seen in the number of lines that are very close to each other for an inclination of 30 degrees while for an inclination of 60 degrees these lines are separated, which means a lower radial recirculation rate. This phenomenon is due to the fact that the steeper the inclination of the reactor, the radial component of gravity decreases, so the fluids tend to generate weaker flow patterns in the radial plane.

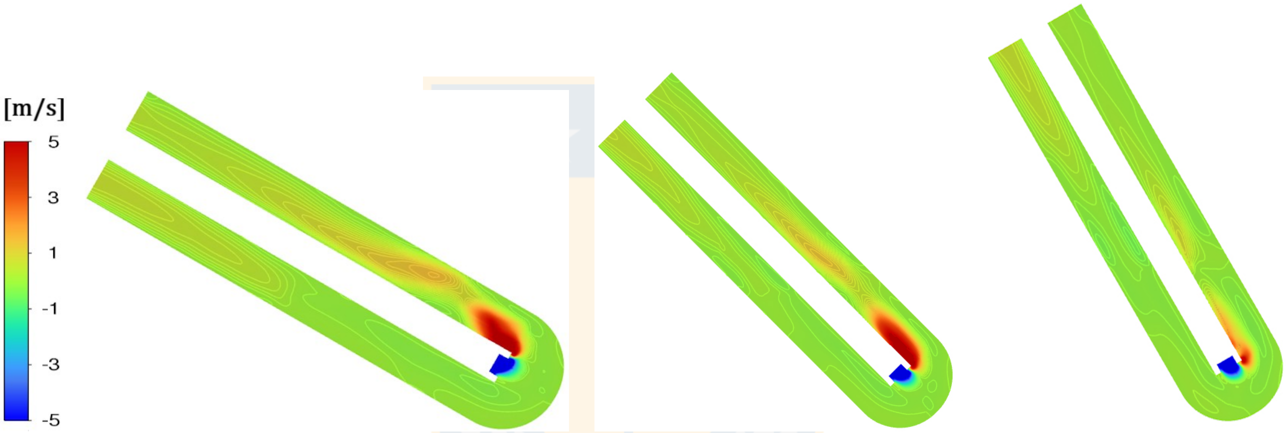

(a) θ=30 degrees. (b) θ=45 degrees. (c) θ=60 degrees.

Figure 4.35: Time-averaged axial velocity. The gas raises slower as the inclination angle increases.

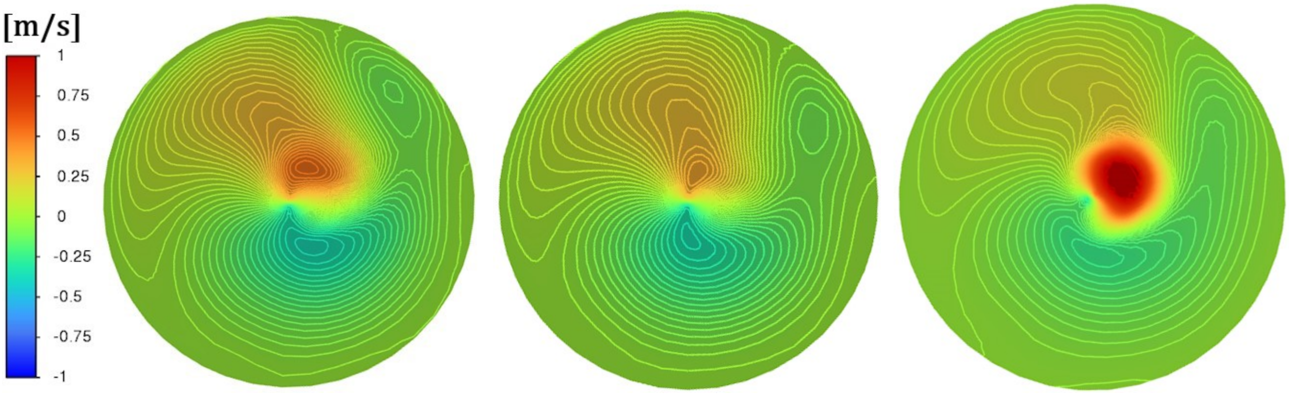

(a) θ=30 degrees. (b) θ=45 degrees. (c) θ=60 degrees.

Figure 4.36: Time-averaged radial velocity. The radial flow patterns get weaker as the inclination angle increases.

5 Conclusions

This study investigated the hydrodynamic behavior of a combined Top-Blown Rotary Converter (TBRC) - Top-Submerged-Lance (TSL) model using Computational Fluid Dynamics (CFD) simulations. The particular characteristics of a TBRC reactor, rotational vessel and inclination, were integrated into a previous TSL computational model. The following conclusions can be drawn:

- **Impact of Operational Parameters**:
  - *Gas flow rate*: The gas flow proved to have the most noticeable impact on the increase of the gas-liquid interface, it also generated a stronger recirculation throughout the crucible, however, decreased the bubble frequency and increased the splashing of the slag.
  - *Lance Immersion Depth*: Increasing lance penetration significantly enhanced bubble frequency and gas-liquid interface but resulted in higher splashing and reduced recirculation at the bottom of the crucible.
  - *Rotation Speed*: Higher rotation speeds improved recirculation patterns and reduced stagnant zones, but excessive speeds increased velocity magnitude along the wall and reduced the gas-liquid interface area.
  - *Inclination Angle*: Inclination angles closer to a TSL configuration resulted in a significant increase in bubble frequency and total gas-liquid interface, however splashing is also increased and radial recirculation is slightly lower.
- **Hydrodynamic Insights**:
  - The study confirmed that gas flow rate play a major role enhancing turbulence and flow patterns, with a proportional relationship between flow rate and gas-liquid interface area.
  - Rotation motion in TBRC reactors was shown to create unique flow patterns not observed in TSL reactors, demonstrating the advantage of combining rotation and lance-submerged based systems.
  - Bubble dynamics is highly influenced by lance penetration, rotation and inclination, and by comparing with literature and other studies, it is confirmed that surface tension also plays a major role.
- **Contributions to Reaction Rates**:
  - Increasing the total interface area, more intense recirculation patterns, and the elimination of stagnant zones directly affect reduction reactions. This is because more intense recirculation patterns ensure that the reactants are in constant contact with the active surfaces

where the reactions occur. Additionally, the reduction of the metal oxide involves the mass transfer from the gas to the liquid phase; a larger interface area facilitates mass transfer, and turbulent flows increase the renewal of the boundary layers of the interface, so mass transport will not be limited by diffusion. Finally, avoiding stagnant zones increases the exposure of the reducing gas to the metal oxides, increasing the probability of reaction and thereby the total conversion.

- **Contributions to Reactor Design**:
  - Although mechanical damage to the crucible wall or lance wear was not directly studied, the high velocities along the wall, excessive splashing, and elevated axial speeds are parameters closely linked to such effects. This emphasizes the importance of balancing operational efficiency with structural integrity in reactor design.
- **Contributions to Reactor safety**:
  - Lance positions very close to the bottom of the crucible or small gas flows create small recirculation patterns or can even lead to stagnation zones, which in case of containing unburned fuel can trigger explosions.
- **Limitations and Future Work**:
  - While this study focused on hydrodynamic behavior, incorporating chemical reactions in future models would provide a more comprehensive understanding.
  - Laboratory or pilot-scale experiments are necessary to confirm and validate the results of the simulations.

Bibliography

[1] NOAA Global Monitoring Laboratory. Trends in atmospheric carbon dioxide, dec 2024.

[2] World Economic Forum. Net-Zero Industry Tracker: 2024 Edition, dec 2024. Accessed: Dec. 2024.

[3] International Energy Agency (IEA). World energy outlook 2024. Technical report, International Energy Agency, 2024. Accenture calculations based on IEA data. Accessed: Dec. 2024.

[4] International Energy Agency (IEA). Emissions measurement and data collection for a net zero steel industry. Technical report, International Energy Agency, 2024. Accessed: Dec. 2024.

[5] International Aluminium Institute (IAI). Greenhouse gas emissions – aluminium sector. Technical report, International Aluminium Institute, 2023. Accenture analysis based on IAI data. Accessed: Dec. 2024.

[6] Mission Possible Partnership (MPP). Making net-zero steel possible. Technical report, Mission Possible Partnership, 2022. Accessed: Oct. 2024.

[7] Fathi Habashi, editor. *Handbook of Extractive Metallurgy: Volume I: The Metal Industry Ferrous Metals*. Wiley-VCH, Weinheim, Germany, 1997. ISBN 978-3-527-29598-8.

[8] C.G. Anderson. Pyrometallurgy. In *Reference Module in Materials Science and Materials Engineering*. Elsevier, 2016. ISBN 978-0-12-803581-8. doi: https://doi.org/10.1016/B978-0-12-803581-8.03609-2.

[9] Allen Yushark Fosu, Danièle Bartier, Frédéric Diot, and Ndue Kanari. Insight into the extractive metallurgy of tin from cassiterite. *Materials*, 17(13), 2024. ISSN 1996-1944. doi: 10.3390/ma17133312.

[10] Elmira Moosavi-Khoonsari and Sina Mostaghel. Thermodynamic assessment of tin-smelting from cassiterite concentrates. *Canadian Metallurgical Quarterly*, 63(3):901–914, 2024. doi: 10.1080/00084433.2023.2266209.

[11] S.R. Chandrashekar. *The Recovery of Tin from Slags by Gaseous Reduction and Fuming*. PhD thesis, University of London, London, UK, December 1977.

[12] Metso's Outotec. Kaldo l furnace. Technical report, Metso Corporation, Helsinki, Finland, 2024. URL `https://www.metso.com`. Document outlining the Kaldo L Furnace technology and specifications.

[13] Fathi Habashi, editor. *Handbook of Extractive Metallurgy: Volume II: Primary Metals, Sec-*

ondary Metals, Light Metals. Wiley-VCH, Weinheim, Germany, 1997. ISBN 978-3-527-29598-8.

[14] Avinash Kandalam, Markus A. Reuter, Michael Stelter, Markus Reinmöller, Martin Gräbner, Andreas Richter, and Alexandros Charitos. A review of top-submerged lance (tsl) processing—part i: Plant and reactor engineering. *Metals*, 13(10), 2023. ISSN 2075-4701. doi: 10.3390/met13101728.

[15] R. Byron Bird, Warren E. Stewart, and Edwin N. Lightfoot. *Transport Phenomena*. John Wiley & Sons, New York, second edition, 2002.

[16] Daniele Obiso, Markus Reuter, and Andreas Richter. Cfd investigations of bath dynamics in a pilot-scale tsl furnace. *Metallurgical and Materials Transactions B*, 52, 07 2021. doi: 10.1007/s11663-021-02233-3.

[17] Mark E. Schlesinger, Matthew J. King, Kathryn C. Sole, and William G. Davenport. *Extractive Metallurgy of Copper*. Elsevier, Oxford, UK, fifth edition, 2011.

[18] D Obiso, S Kriebitzsch, M Reuter, and B Meyer. The importance of viscous and interfacial forces in the hydrodynamics of the top-submerged-lance furnace. *Metallurgical and Materials Transactions B*, 50:2403–2420, 2019.

[19] Daniele Obiso, M Akashi, S Kriebitzsch, B Meyer, M Reuter, S Eckert, and A Richter. Cfd modeling and experimental validation of top-submerged-lance gas injection in liquid metal. *Metallurgical and Materials Transactions B*, 51(4):1509–1525, 2020.

[20] Manuel Pérez-Tello, María M Salazar-Campoy, and Óscar Rodríguez-Hoyos. Cold-model study on the maximum penetration distance of the injection lance in a kaldo furnace. *Mining, Metallurgy & Exploration*, 37(3):943–954, 2020.

[21] Jindi Huang, Dou Zhang, Jing Li, Jinlong Zhong, Haoling Huang, Fupeng Liu, Mingzhou Li, and Songlin Zhou. A water model study on mixing behaviour in a kaldo furnace using acid–base neutralization decolourization method combined with rgb-based image analysis. *Chemical Engineering Research and Design*, 2024.

[22] Albrecht Voigt. Modellierung von gas-flüssig-systemen am beispiel der sno2-reduktion mittels h2. Master's thesis, Technische Universität Bergakademie Freiberg, March 2024. Diplomarbeit.

[23] Hongliang Zhao, Yadong Xiao, Fengqin Liu, and Hong Yong Sohn. Computational fluid dynamics simulation of gas–matte–slag three-phase flow in an isasmelt furnace. *Metallurgical and Materials Transactions B*, 52, 08 2021. doi: 10.1007/s11663-021-02290-8.

[24] Joel H. Ferziger, Milovan Perić, and Robert L. Street. *Computational Methods for Fluid Dynamics*. Springer, Cham, Switzerland, fourth edition, 2020.

[25] Aurubis AG. Corporative aurubis profile. `https://www.aurubis.com/en/`, 2024.

[26] Aurubis AG. The kayser recycling system (krs): Efficient multi-metal recycling technology. https://www.aurubis.com, 2024.

[27] Grétar Tryggvason, Ruben Scardovelli, and Stéphane Zaleski. *The volume-of-fluid method*, page 95–132. Cambridge University Press, 2011.

[28] ANSYS Inc. *ANSYS Fluent User's Guide*. ANSYS Inc., Canonsburg, PA, USA, release 2024 r2 edition, 2024.

[29] Metso. Kaldo furnace technical data. https://www.metso.com/portfolio/kaldo-furnace/, 2024. Accessed: 2024-12-22.

[30] Megumi Akashi, Olga Keplinger, Natalia Shevchenko, Sten Anders, Markus Reuter, and Sven Eckert. X-ray radioscopic visualization of bubbly flows injected through a top submerged lance into a liquid metal. *Metallurgical and Materials Transactions B*, 51, 10 2019. doi: 10.1007/s11663-019-01720-y.

[31] Avinash Kandalam, Markus A Reuter, Michael Stelter, Markus Reinmöller, Martin Gräbner, Andreas Richter, and Alexandros Charitos. A review of top submerged lance (tsl) processing—part ii: Thermodynamics, slag chemistry and plant flowsheets. *Metals*, 13(10):1742, 2023.

[32] R. Clift, J.R. Grace, and M.E. Weber. *Bubbles, Drops, and Particles*. Academic Press, 1978. ISBN 9780121769505.

[33] Lingling Cao, Yannan Wang, Zhongfu Cheng, Hongming Wang, and Guirong Li. Bubble formation and surface sloshing in the tsl flow with a viscous liquid. *Jom*, 74(12):4920–4929, 2022.

[34] Karine Loubière and Gilles Hébrard. Influence of liquid surface tension (surfactants) on bubble formation at rigid and flexible orifices. *Chemical Engineering and Processing: Process Intensification*, 43(11):1361–1369, 2004. ISSN 0255-2701. doi: https://doi.org/10.1016/j.cep.2004.03.009. Special Issue on Gas-Liquid and Gas-Liquid-Solid Reactor Engineering.

[35] Javad Eshraghi, Erfan Kosari, Pooria Hadikhani, Ali Amini, Mehdi Ashjaee, and Pedram Hanafizadeh. Numerical study of surface tension effects on bubble detachment in a submerged needle. In *8th International Conference on Computational and Experimental Methods in Multiphase and Complex Flow (WESSEX)*, 04 2015.

Appendices

Appendix A: Raw Data

To generate the graphs presented in the results section, data was extracted for 4 seconds of simulation. The first 0.5 seconds were discarded as the fluids were transitioning out of inertia, and the remaining 3.5 seconds were time-averaged. The following graphs correspond to the ”raw data” extracted directly from the ANSYS Fluent program.

Splashing height

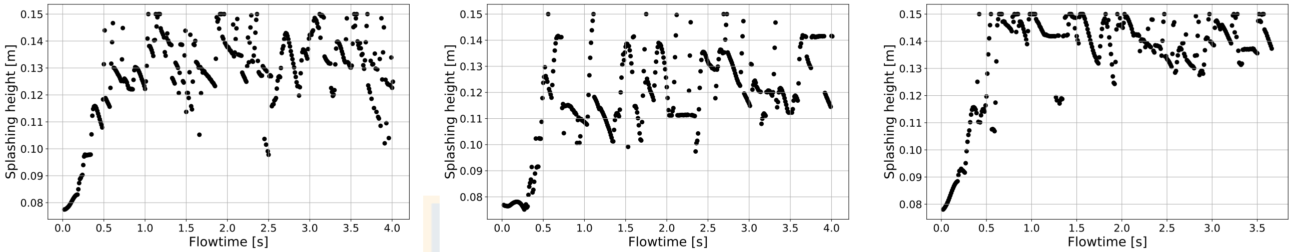

(a) Original TBRC 45 case.

(b) Gas flow rate decreased by 50%.

(c) Gas flow rate increased by 50%.

Figure 1: Raw data: Splashing Height.

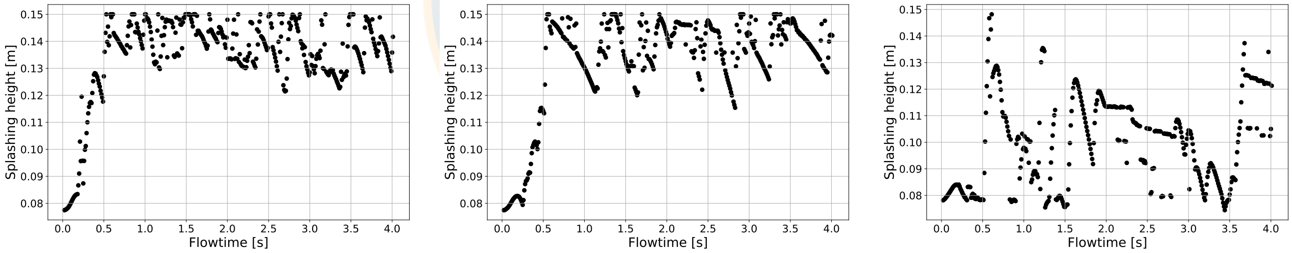

(a) Rotation speed: 48 rpm.

(b) Rotation speed: 143 rpm.

(c) d/D = 0.733.

Figure 2: Raw data: Splashing Height.

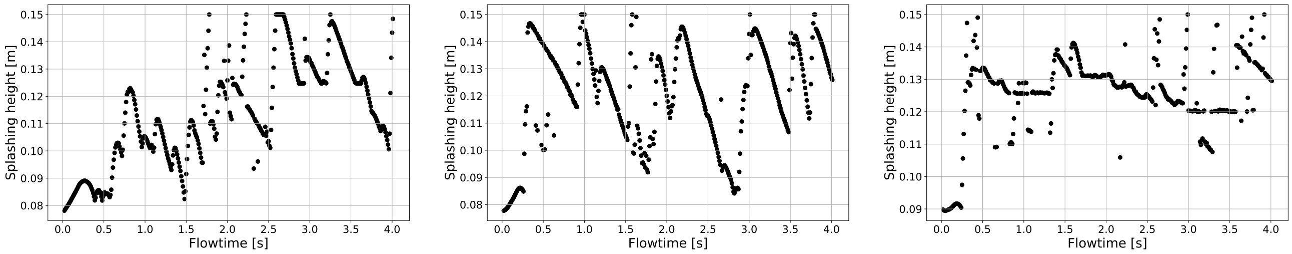

(a) d/D = 0.8.

(b) d/D = 0.933.

(c) Inclination: 30 degrees.

Figure 3: Raw data: Splashing Height.

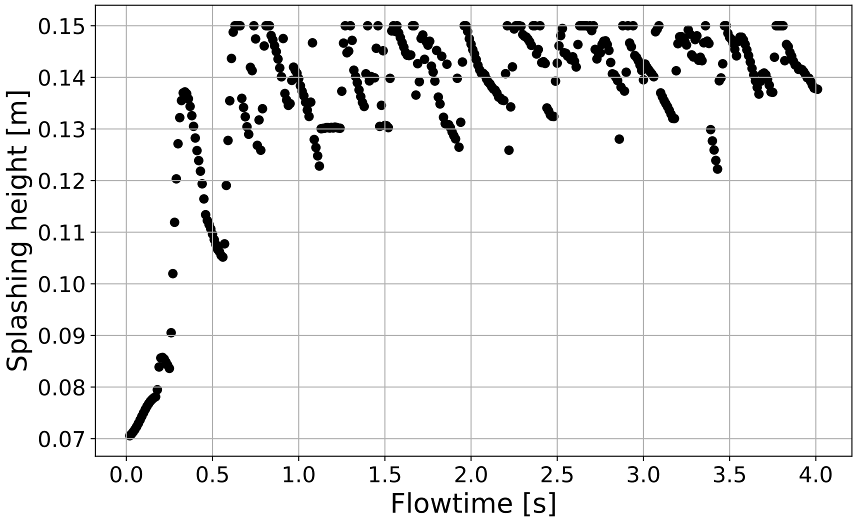

Figure 4: Raw data: Splashing Height. Inclination: 60 degrees.

Interface area

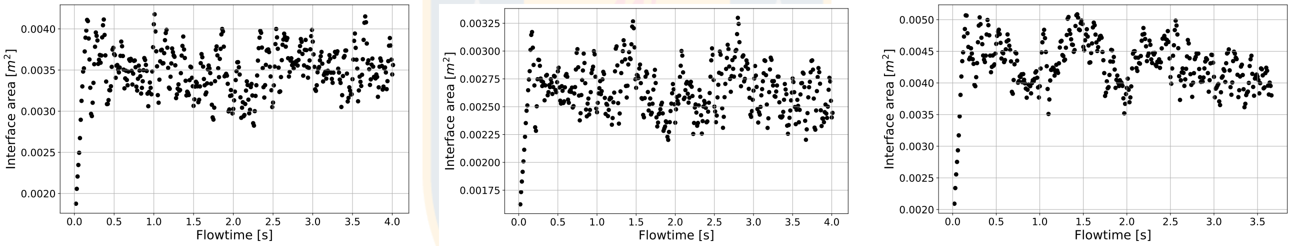

(a) Original TBRC 45 case.

(b) Gas flow rate decreased by 50%.

(c) Gas flow rate increased by 50%.

Figure 5: Raw data: Interface Area.

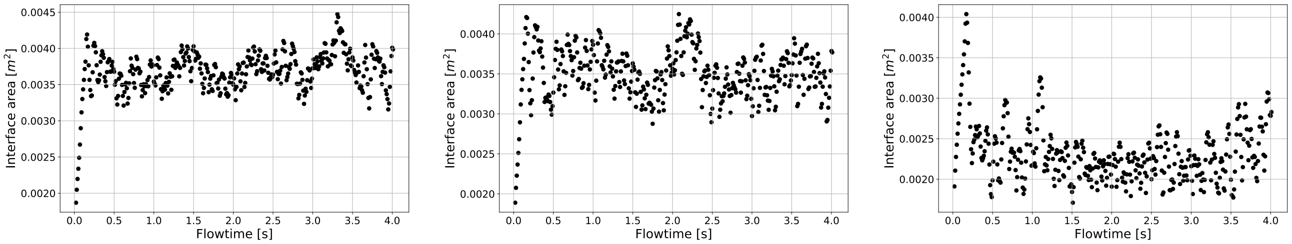

(a) Rotation speed: 48 rpm.

(b) Rotation speed: 143 rpm.

(c) d/D = 0.733.

Figure 6: Raw data: Interface Area.

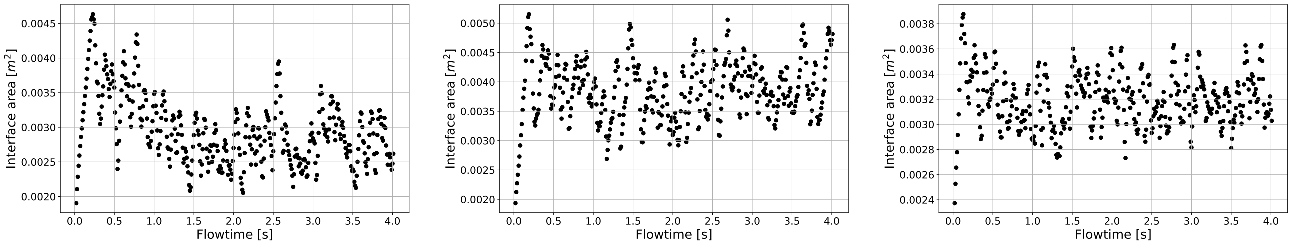

(a) d/D = 0.8.

(b) d/D = 0.933.

(c) Inclination: 30 degrees.

Figure 7: Raw data: Interface Area.

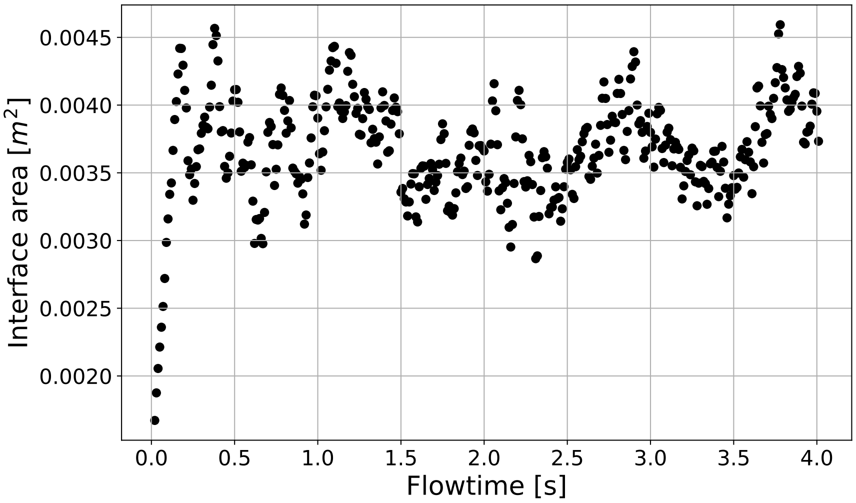

Figure 8: Raw data: Interface Area. Inclination: 60 degrees.

Bubble frequency:

The information provided by ANSYS Fluent corresponds to the time signal, as explained in Section 4.2.3. The following graphs represent the data delivered directly by ANSYS Fluent (without further manipulation).

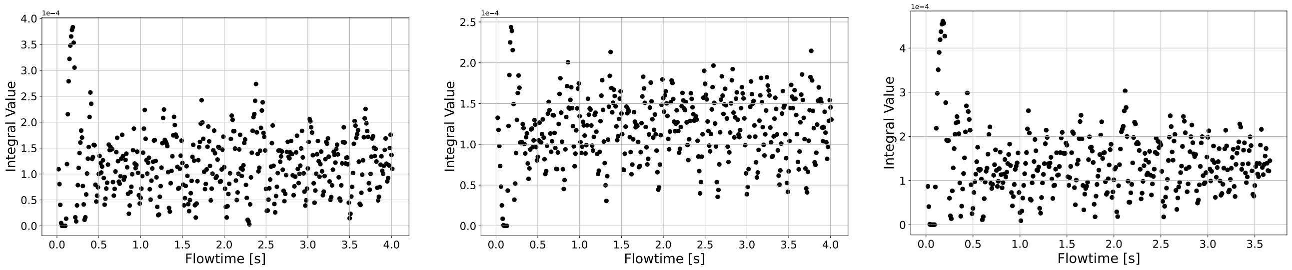

(a) Original TBRC45 case.

(b) Gas flow rate decreased by 50%.

(c) Gas flow rate increased by 50%.

Figure 9: Raw data: Time Evolution of Integral Values.

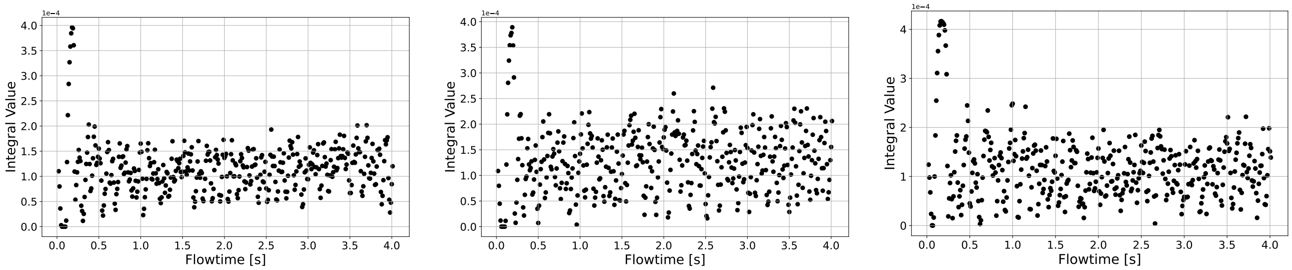

(a) Rotation speed: 48 rpm. (b) Rotation speed: 143 rpm. (c) d/D = 0.733.

Figure 10: Raw data: Time Evolution of Integral Values.

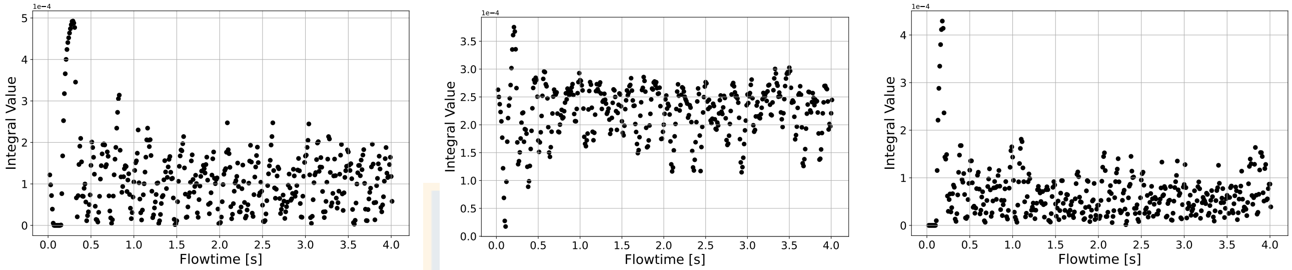

(a) d/D = 0.8 (b) Inclination: 30 degree. (c) Inclination: 60 degree.

Figure 11: Raw data: Time Evolution of Integral Values.

Appendix B: Standard Error Calculation

To calculate the standard error represented by the bars in Figures 4.16-4.19, 4.21, 4.22, 4.25, and 4.26, the standard error was computed. To illustrate the procedure, an example of the calculation for the standard error of the Splashing Height for the original case (Figure 1(a)) is shown.

Step 1: Data Table

The data of Figure 1. (a) is tabulated below:

Time (s)	Splashing Height (m)
0.5	0.128898844
0.51	0.141442999
0.52	0.116318725
0.53	0.115730956
0.54	0.115061834
0.55	0.114434011
0.56	0.113832116
0.57	0.113139920
0.58	0.120116614
0.59	0.129100755

(Note: Only a subset of the data is shown for brevity.)

Step 2: Calculate the Mean ($\bar{x}$)

The mean ($\bar{x}$) is calculated as:

$$\bar{x} = \frac{\sum_{i=1}^{n} x_i}{n}$$

Where:

- x_i: Each individual value of the splashing height.
- n: Total number of observations.

Step 3: Calculate the Standard Deviation (σ)

Using the mean, the standard deviation is calculated as:

$$\sigma = \sqrt{\frac{\sum_{i=1}^{n}(x_i - \bar{x})^2}{n-1}}$$

Where:

- $x_i - \bar{x}$: The difference between each value and the mean.
- $(x_i - \bar{x})^2$: The square of these differences.
- $n-1$: Degrees of freedom for the sample.

Step 4: Determine the Sample Size (n)

The sample size corresponds to the total number of data points:

$$n = \text{total number of observations.}$$

Step 5: Calculate the Standard Error

Finally, the standard error of the mean (SEM) is calculated as:

$$\text{SEM} = \frac{\sigma}{\sqrt{n}}$$

Where:

- σ: Sample standard deviation.
- n: Sample size.

Final Result

The calculated standard error for this data is:

$$\text{SEM} = 0.00115 \text{ meters.}$$

The same procedure was applied for all the datasets presented in the Chapter 4.

Resumen FI

UNIVERSIDAD DE CONCEPCION – FACULTAD DE INGENIERIA
RESUMEN DE MEMORIA DE TITULO

Departamento	Departamento de Ingeniería
Carrera	Ingeniería Civil Química
Nombre del memorista	Maximiliano Antonio Sepúlveda Irarrázabal
Título de la memoria	CFD-based studies and model development for a Top-Blown Rotary Converter
Fecha de la presentación oral	
Profesor(es) Guía	Diego Becerra y Andreas Richter
Profesor(es) Revisor(es)	Andrés Mejía
Concepto	
Calificación	

Resumen

Las simulaciones computacionales son una herramienta eficaz para estudiar fenómenos complejos, especialmente útil en investigación y creación de prototipos por su bajo costo y alta precisión. Este estudio presenta un modelo computacional de un reactor metalúrgico TBRC basado en un modelo TSL, ambos empleados en la industria de metales no ferrosos y considerados opciones sostenibles.

El proposito de este trabajo es entender la hidrodinamica del modelo a traves de un estudio parametrico de los parametros operacionales para ello se utilizó Ansys Fluent con el modelo "Volume of Fluid" (VOF) acoplado al modelo de turbulencia k-ω SST. Se analizaron variables como el área de la interfaz gas-líquido, frecuencia de burbujeo, y splashing, complementadas con imágenes instantáneas y promediadas en el tiempo.

Los resultados muestran que la penetración de la lanza incrementa la superficie gas-líquido y afecta la frecuencia de burbujas, pero debilita los patrones de recirculación, favoreciendo zonas de estancamiento. La rotación mejora la recirculación, especialmente en la base del reactor y la inclinación disminuye la interacción gas-liquido.